Title
12C AND 8Be PRODUCTION IN 12C+208Pb COLLISIONS

Authors
Bice, A.N.
Shotter, A.C.
Cerny, J.

Publication Date
1982-05-01

Lawrence Berkeley Laboratory
UNIVERSITY OF CALIFORNIA

Submitted to Nuclear Physics

$^{12}C^{*}$ AND ^{8}Be PRODUCTION IN $^{12}C+^{208}Pb$ COLLISIONS

A.N. Bice, A.C. Shotter, and Joseph Cerny

May 1982

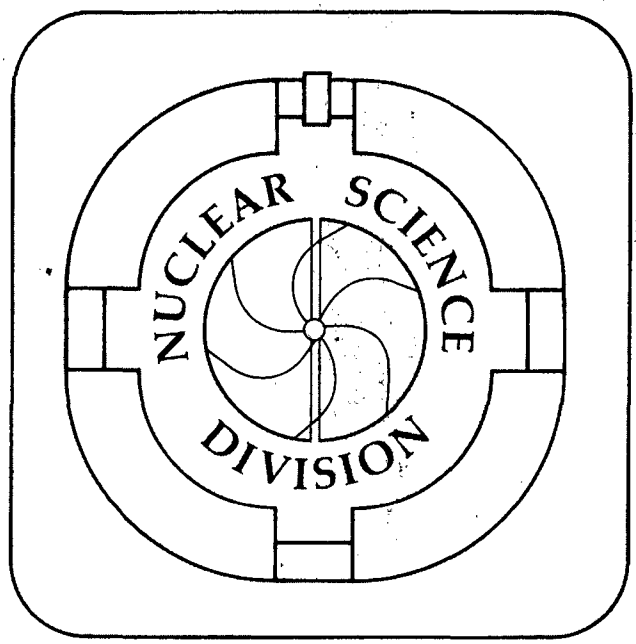

Prepared for the U.S. Department of Energy under Contract DE-AC03-76SF00098

DISCLAIMER

$^{12}C^{*}$ and ^{8}Be Production in $^{12}C+^{208}Pb$ Collisions

A. N. Bice, A. C. Shotter, and Joseph Cerny

Department of Chemistry
University of California, and
Lawrence Berkeley Laboratory
Berkeley, CA 94720

This work was supported by the Director, Office of Energy Research, Office of High Energy and Nuclear Physics of the U.S. Department of Energy under contract No. DE-AC03-76SF00098.

$^{12}C^*$ and ^{8}Be Production in $^{12}C+^{208}Pb$ Collisions[‡]

A. N. Bice,[†] A. C. Shotter[††] and Joseph Cerny

Department of Chemistry
University of California, and
Lawrence Berkeley Laboratory
Berkeley, CA 94720

Abstract: The mechanisms involved in the production of fast α-particles in ^{12}C induced reactions have been studied for the $^{12}C+^{208}Pb$ system at the bombarding energies of $E_{^{12}C}$=132, 187 and 230 MeV. Absolute cross sections for the reactions $^{208}Pb(^{12}C,^{12}C^*\rightarrow\alpha+^{8}Be)$, $^{208}Pb(^{12}C,^{8}Be(g.s.))$ and $^{208}Pb(^{12}C,^{8}Be(2.94\ MeV))$ have been determined by coincidence measurement of two or three correlated α-particles. Inclusive α-particle production cross sections were also measured at $E_{^{12}C}$=187 MeV. It is found that the inelastic process $(^{12}C,^{12}C^*\rightarrow\alpha+^{8}Be)$ does not contribute significantly to fast α-particle production but that the production of ^{8}Be by projectile fragmentation is an important source of α-particles. At the highest bombarding energy (230 MeV) it appears that the $^{12}C\rightarrow 3\alpha$ fragmentation reaction becomes more prominent at the expense of the $^{12}C\rightarrow\alpha+^{8}Be$ fragmentation channel.

[NUCLEAR REACTIONS: $^{208}Pb+^{12}C$, E=132, 187 and 230 MeV; measured $d^2\sigma/dEd\Omega(E_\alpha)$, $d^2\sigma/dEd\Omega(E_{^{8}Be(g.s.)})$, $d^2\sigma/dEd\Omega(E_{^{8}Be(2.94\ MeV)})$, $d^2\sigma/dEd\Omega(E_{^{12}C^*})$; deduced contribution of projectile breakup to fast α-particle cross section.]

[†]Present address: U.S. NRC/ACRS, Washington, D.C. 20555.
[††]Permanent address: Physics Department, University of Edinburgh, Edinburgh, EH93JZ, United Kingdom.

I. Introduction

A prominent feature of reactions involving very asymmetric heavy-ion systems at bombarding energies of ~8-20 MeV/nucleon is the copious production of noncompound α-particles with mean velocities close to that of the projectile. This reaction characteristic was noted as early as 1961 by Britt and Quinton [1] who suggested that the principal process involved in the production of beam velocity α-particles was the breakup of the incident projectile in an interaction with the surface of the target nucleus. It was not until the measurements of Galin et al. [2] that interest was renewed in determining the origin of the fast alpha particles. Measurements of α-γ coincidences by Inamura et al. [3] indicated that many of the fast α-particles are produced in reactions that can be regarded as incomplete fusion/massive transfer, that is, only a portion of the projectile is captured or fuses with the target nucleus. Additional experimental investigations [4-12] have established conclusively the existence of an incomplete fusion reaction mechanism in the interaction of ^{6}Li to ^{16}O projectiles with heavy targets at bombarding energies of ~7-17 MeV/nucleon. Furthermore, evidence has been obtained that central collisions do not, in general, participate in incomplete fusion reactions and that this mass transfer process occurs over a narrow range of entrance channel angular momenta, L, beginning near the critical angular momentum, L_{crit}, for complete fusion. Finally, it is found that the

average angular momentum transferred to the target nucleus in the capture of projectile fragments increases linearly with captured mass.

K. Siwek-Wilczynska et al. [9,10] recently proposed a simple model of incomplete fusion reactions. From a study of α-γ coincidences resulting from the dominant incomplete fusion reactions $^{160}Gd(^{12}C,\alpha)$ and $^{160}Gd(^{12}C,2\alpha)$ at bombarding energies of 7.5-16.7 MeV/A, Siwek-Wilczynska et al. concluded that incomplete fusion reactions are simply an extension of the fusion process to angular momentum values above the initial system's critical angular momentum. Each virtual projectile fragment was assumed to carry a part of the total angular momentum in proportion to its mass number. The capture of a projectile fragment by the target nucleus was postulated to occur within sharp L-windows which are defined in relation to the critical angular momentum for the target plus fragment system. Above a bombarding energy of approximately 15 MeV/A, the balance of the nuclear, Coulomb and centrifugal forces is no longer sufficient for the capture of a projectile fragment to occur; therefore, the cross section for binary incomplete fusion processes must begin to decrease while that for multibody fragmentation processes increases in magnitude.

More recently the generalized concept of critical angular momentum was extended by J. Wilczynski et al. [12] with the proposal of a sum rule model that permits one to predict absolute cross sections for all incomplete fusion channels as well as for

complete fusion. In this model, reaction channel cross sections are strongly dependent upon 1) a phase space factor which has an exponential dependence on the ground state Q-value, Q_{gg}, and 2) transmission coefficients which create an L-window effect.

This sum rule model was found to predict rather well the binary reaction cross sections resulting from incomplete fusion reactions in the $^{14}N+^{159}Tb$ system and the excitation functions for the two main incomplete fusion channels in the $^{12}C+^{160}Gd$ system. However, it should be noted that for the $^{12}C+^{160}Gd$ system over bombarding energies of 90-200 MeV, only 20-40% of the measured singles α-particles resulted from the incomplete fusion reaction channels ($^{12}C,\alpha$) and ($^{12}C,2\alpha$). Above about 15 MeV/A for the $^{12}C+^{160}Gd$ system, the multibody fragmentation channel is predicted to become prominent. Presumably the multibody fragmentation channel is responsible for the production of large amounts of fast-alpha particles via the $^{12}C \rightarrow 3\alpha$ reaction, although the relative strength of this reaction channel compared to other multibody channels is not provided by the sum rule model. Furthermore, this simple model does not contain any allowance for projectile spectroscopic properties nor does it predict any final state features such as particle angular distributions, particle-particle correlations and particle energy spectra. Thus, for some systems (most notably the $^{12}C+^{160}Gd$ system), the incomplete fusion sum rule reasonably predicts the incomplete fusion cross sections but it only suggests the source of the remaining 80% or so of singles α-particles. It is of

interest then to determine if the $^{12}C \rightarrow 3\alpha$ channel is a large contributor of fast alpha particles. (Recent particle-γ measurements of Hsu et al. [13] found evidence for the onset of a multibody process with a ^{20}Ne beam at ~17 MeV/A bombarding energy.)

In this paper we present results of an investigation into fast α-particle production via the production of ^{8}Be(g.s.), ^{8}Be(2.94 MeV) and excited ^{12}C reaction products from the $^{12}C+^{208}Pb$ system at ^{12}C bombarding energies of 132, 187 and 230 MeV. Absolute cross sections have been obtained for the reactions $^{208}Pb(^{12}C,^{12}C^{*}_{\rightarrow\alpha+^{8}Be})$, $^{208}Pb(^{12}C,^{8}Be(g.s.))$ and $^{208}Pb(^{12}C,^{8}Be(2.94\ MeV))$ by coincident measurement of three α-particles or two α-particles for $^{12}C^{*}$ and ^{8}Be detection, respectively. By folding in the probability of detecting correlated particles, the absolute production cross sections were determined which were then compared with the measured singles α-particle cross section at 187 MeV ^{12}C bombarding energy. From this comparison, further information could be obtained about the reaction channels important in fast α-particle production.

II. ^{12}C Dissociation Considerations

^{12}C induced reactions on heavy targets have been studied by several groups [1,9,10,12,14-16]. Measurements of the angular distributions, energy spectra and differential cross sections of alpha particles emitted in the bombardment of Au and

Bi targets by 126 MeV ^{12}C nuclei permitted Britt and Quinton [1] to conclude that a majority of the alpha particles observed (some 900 mb) resulted from a direct process, most probably breakup of the incident projectile. Eyal et al. [14] estimated that about 150 mb of unbound ^{8}Be nuclei are produced in the $^{12}C+^{197}Au$ reaction at 125 MeV bombarding energy. Kozub et al. [15] complemented the work of Eyal et al. by measuring the cross section for the production of $^{8}Be(0^{+},g.s.)$ nuclei in the $^{12}C+^{197}Au$ reaction at 126 MeV. It was determined that about 37 mb of $^{8}Be(g.s.)$ was produced which indicated strongly that a substantial amount of cross section existed for the production of excited states of ^{8}Be. As mentioned above, measurements of the cross section of incomplete fusion reactions for the $^{12}C+^{160}Gd$ system at bombarding energies of 90-200 MeV permitted Siwek-Wilczynska et al. [9,10] to suggest that the projectile fragmentation channel, $(^{12}C,3\alpha)$, is the dominant source of fast alpha particles, especially at the increased bombarding energies.

It is clear that several reaction mechanisms might explain the observations noted above. An intuitive understanding of these observations is possible with a simple model of limiting angular momentum [17]. As pointed out by Brink [18], transfer reactions between heavy ions at energies well above the Coulomb barrier have large transfer probabilities only if certain kinematic conditions are satisfied. In particular, the transfer cross section will be the largest when the transferred particle retains nearly the velocity of the projectile. Semiclassically, this implies that

the angular momentum transferred to the heavy residual nucleus is given by $mvR/\hbar$ where m is the transferred mass, R is the "radius" at which the transfer occurs and v is the relative velocity of the projectile and target. For some velocity v, the attractive interaction between the transferred particle and the target nucleus will no longer be sufficient to capture the transferred fragment. The fragment escapes before its angular momentum and energy can be absorbed by the target system.

Figure 1 shows the transferred angular momentum as a function of the transferred fragment mass for the three ^{12}C bombarding energies employed in this work. The dashed line represents the critical angular momentum for each fragment-target system as calculated by Wilczynski [19]. It is seen that at the lowest energy, 132 MeV, transfer occurs without exceeding L_{crit}. At 187 MeV up to six or seven nucleons can be transferred before L_{crit} is surpassed. Thus, transfer of a ^{8}Be nucleus may not be possible, suggesting that a large increase in ^{8}Be production may occur between 132 and 187 MeV. At the highest bombarding energy of 230 MeV, transfer of four nucleons just about exceeds L_{crit}. Thus, at the higher energies nucleon transfer turns into a fragmentation process.

An extension of these simple arguments, in an empirical way, was presented by Wilczynski et al. [12]. Figure 2 presents the incomplete fusion calculations as discussed in Section I for the $^{12}C+^{208}Pb$ system. Parameters employed were determined in a similar fashion to those in reference 12. Figure 2a indicates

that, for lower angular momenta, the complete fusion channel has the largest probability factor (see the factor on the ordinate axis). At higher angular momentum values the incomplete fusion (massive transfer) channels ($^{12}C,\alpha$) and ($^{12}C,2\alpha$) become evident. Predicted cross section trends are shown in fig. 2b.

The predictions shown in fig. 2 can be seen to be rather similar to those made for the $^{12}C+^{160}Gd$ system [12]. In this latter case, such calculations adequately reproduced the excitation functions for the measured incomplete fusion channels $^{160}Gd(^{12}C,\alpha)$ and $^{160}Gd(^{12}C,2\alpha)$, which were found to account for 20-40% of the inclusive alpha particles. Thus, it is expected that the $^{12}C+^{208}Pb$ system has a similar contribution of fast alpha particles from the incomplete fusion channels $^{208}Pb(^{12}C,\alpha)$ and $^{208}Pb(^{12}C,2\alpha)$.

Another prominent feature of fig. 2 is the cross section prediction for the multibody fragmentation channel, denoted ($^{12}C,^{12}C'$). A rapid rise in the fragmentation cross section is expected between ~130 MeV and ~230 MeV. Owing to the fact that the three-alpha breakup threshold has the most positive Q-value relative to other fragmentation channels, it is expected (cf. 20,21) that a large portion of the ($^{12}C,^{12}C'$) curve will be composed of three-alpha production cross section. However, as previously noted, the incomplete fusion sum rule model does not provide this information.

The production of fast alpha particles from the breakup of the ^{12}C projectile nucleus can be viewed as occurring in

several ways: i) the (^{12}C,$^{12}C^{*}\rightarrow\alpha+^{8}Be$) reaction, ii) the ($^{12}C$,$\alpha+^{8}Be$) reaction and iii) the (^{12}C,$\alpha+\alpha+\alpha$) reaction. Reaction process i) represents the excitation of the ^{12}C projectile via an inelastic scattering process and its subsequent decay into an α and a ^{8}Be nucleus. ^{12}C excited states above 7.4 MeV can decay sequentially into $\alpha+^{8}Be$ fragments. Typical inelastic scattering cross sections are on the order of millibarns and it is expected that mechanism i) should have a similar yield. The mechanism of reaction ii) is a direct fragmentation of the ^{12}C projectile into an alpha particle and a ^{8}Be nucleus. Presumably the relative momentum of the α and the ^{8}Be nuclei in the projectile bound state would influence the final laboratory momenta of the two breakup fragments. The mechanism represented by iii) is also a direct fragmentation process, but one which produces three free alpha particles: no intermediate ^{8}Be nucleus is involved. Note that process i) is indistinguishable from ii) if the level width of the sequentially decaying state in ^{12}C is sufficiently broad. Nonetheless, processes i) and ii) are clearly distinct from iii) since they necessarily involve the production of ^{8}Be nuclei.

Thus, it is of interest to investigate the production of the sequential decay products $^{12}C^{*}$ and ^{8}Be in ^{12}C induced reactions for energies in the range of 10-20 MeV/nucleon. Such measurements, presented below, provide important complementary information to that obtained previously [1,10,14,15].

III. Experimental Technique

^{12}C beams from the Lawrence Berkeley Laboratory's 88-inch cyclotron were used to bombard ^{208}Pb targets which were self-supporting and enriched to ~99%. The $^{12}C+^{208}Pb \rightarrow ^{8}Be$ or $^{12}C^{*}$ reactions were investigated at $E(^{12}C)$=132, 187 and 230 MeV to elucidate further the mechanisms involved in fast α-particle production at these bombarding energies. The detection of ^{8}Be and the unbound $^{12}C^{*}$ products were performed by the coincident detection of two or three alpha particles, respectively.

In the studies presented here, the detection of sequentially decaying reaction products was of principal interest. In kinematically complete experiments the spatial arrangement of particle telescopes can severely restrict or enhance the observation of certain multibody final states. For instance, the detection of sequentially decaying reaction products is enhanced when the particle telescopes are separated by an angular amount that is similar to the maximum opening angle of the decay fragments in the laboratory frame. The detection probability is further enhanced if large solid angle counters are employed. However, large solid angle counters imply poorer energy resolution (due to the dE/dθ). On the other hand, small solid angle counters imply lower coincidence counting rates and a decreased true to random coincidence ratio. Thus, there are several factors which must be considered in selecting a coincidence detection system. These are: 1) the range of opening angles between sequential decay

fragments, 2) the experimental tolerance in energy resolution, 3) the counting rate deemed satisfactory and 4) an acceptable ratio of true to random coincidences.

Given these considerations a reasonable detection system for the observation of $^{8}Be(g.s.)$, $^{8}Be(2.94\ MeV)$ and $^{12}C^{*}$ reaction products is depicted schematically in fig. 3. In its fullest extent, the detection system consisted of three ΔE-E counter telescopes mounted on a movable platform and arranged in a vertical fashion with respect to the normal scattering plane. Particle telescopes labeled 1 and 2 were located symmetrically above and below the scattering plane: i.e., the collimator post between these two telescopes was bisected by the horizontal reaction plane. The third telescope was always located above the reaction plane. Behind each E counter (and not shown in fig. 3) was an E_{rej} counter which vetoed any (generally unexpected) high energy events in which the particle completely traversed the ΔE-E system.

Table 1 lists the pertinent dimensions of the detection system shown in fig. 3. Coincidence events between any pair of telescopes were recorded but simultaneous events in all three were not. Telescope combination 1-2 was most suitable for detecting unbound particles with small decay energies, such as $^{8}Be(g.s.)$ which is unbound by 0.092 MeV, because the two telescopes were separated by only about 3°. This combination was also the most suitable for separating the sequential decay peaks in projected energy spectra due to the velocity addition

effect (cf. fig. 15 and associated discussion below). Telescope combination 1-3 was more suitable for attempting to observe sequential decays of products with large decay energies.

For this detection system the horizontal acceptance angle, as determined by the collimator width, was 3°. However, the effective "horizontal" acceptance angle was slightly larger than this, especially for the telescope combinations 2-3 and 1-3, because the geometry of the system allowed detection of decay events in which the center-of-mass direction of the unbound ejectile is slightly out of the reaction plane. The typical energy resolution was about 400 to 600 keV full width at half maximum (FWHM) depending upon the reaction.

For the $^{12}C^{*}{}_{\rightarrow\alpha+^{8}Be}$ investigation, it was necessary to detect two α-particles in one particle telescope in coincidence with a third α-particle in another telescope. If two α-particles enter the same telescope, each with about the same kinetic energy, they will identify together as a ^{7}Li event [22]. $^{12}C^{*}$ events were identified then as an $\alpha+^{7}Li$ coincidence. (For the Pb target, a gate on the $\alpha+^{8}Be$ total energy around the ^{12}C quasielastic peak served to remove any real $\alpha+^{7}Li$ coincidences due to the Q-value difference.)

The calculation of the absolute production cross sections for the sequentially decaying unbound reaction products, $^{8}Be(g.s.)$, $^{8}Be(2.94\ MeV)$ and $^{12}C^{*}{}_{\rightarrow\alpha+^{8}Be}$, was performed by folding the detection probabilities into the measured double differential cross sections, $d^{2}\sigma/d\Omega_{\alpha_1}d\Omega_{\alpha_2}$ and $\frac{d^{2}\sigma}{d\Omega_{^{8}Be}d\Omega_{\alpha}}$.

A Monte Carlo type program was used to calculate the detection probabilities. This program allows both a random selection of the $^{12}C^*$ emission angles and the angles for emission of the α and ^8Be projectiles in the $^{12}C^*$ center-of-mass frame. It is assumed that the center of mass emission distribution is isotropic.[23]

Figures 4 and 5 illustrate the detection efficiency of ^8Be(g.s.) and ^8Be(2.94 MeV) nuclei as a function of their total kinetic energy (after decay). The solid angle subtended by each particle telescope is represented by Ω_i and the vertical, center-to-center angular separation of the two telescopes is designated by $\theta_{separation}$. It is evident that, in general, the detection efficiency is small (.2 - 2%) and it is highly dependent upon the fragment's relative energy and the total kinetic energy.

Figures 6 and 7 present the calculated detection efficiencies of $^{12}C^*$(7.6 MeV) and $^{12}C^*$(9.6 MeV) as a function of the total kinetic energy of the three final α-particles. Two curves are shown in figs. 6 and 7. The dashed curve results from the requirement in the Monte Carlo simulation that the two α-particles, which result from the decay of the ^8Be(g.s.) fragment, actually enter the same telescope with the third α-particle entering the opposite telescope. The solid curve represents the efficiency of two telescopes simply detecting the three α-particles, two α's in any one telescope, one α in the other telescope. The solid curve was the one

employed in production cross section determinations. It can be seen that detection efficiencies range from about .9% downward. Table 2 lists the detection efficiencies of excited ^{12}C reaction products with the three telescope geometries employed in these studies. It can be seen that the probability of detecting three alpha particles decreases rapidly with increasing excitation energy of the ^{12}C ejectile and that the detection efficiency depends strongly on the detection configuration and $^{12}C^*$ decay channel. From table 2 it is seen that (for a ^{12}C bombarding energy of 230 MeV) the detection of ^{12}C reaction products excited to levels above ~16 MeV is extremely unlikely. The production of $^{12}C^*$ nuclei at excitation energies above ~16 MeV would therefore not be observed in this study.

All particle-particle coincidence data as well as the single particle inclusive data were recorded event by event on magnetic tape. Off-line analysis was performed by re-sorting the stored binary data with software gates in the necessary particle identification spectra, TAC spectra and energy spectra. A correction for random coincidences was performed by subtracting events which resulted from coincidences between beam bursts from those events which resulted from intra-beam burst coincidences.

Target thicknesses were determined by measurement of the energy reduction of 6.06 MeV and 8.78 MeV α-particles (from a $^{212}Po/^{212}Bi$ α-source) which had passed through the targets. Target thicknesses determined in this manner are estimated to be

accurate to within ±10%. An upper limit on the amount of light contaminants in the ~1.5 mg/cm^2 thick ^{208}Pb targets was established to be 20 μg/cm^2, which contributed a negligible effect to the cross section estimates.

Systematic errors in all cross section determinations are estimated to be no more than about 25% and are primarily due to possible errors in the estimation of the total dead time, the integrated charge, the target thickness and the detection system's solid angle.

IV. Experimental Results and Discussion

Presented below are experimental results concerning the production of α-particles from the ^{12}C+^{208}Pb system at E(^{12}C)=132, 187 and 230 MeV bombarding energy. Part of these results have been reported previously [24].

Figure 8 shows a series of α-particle spectra that resulted from the bombardment of a 1.5 mg/cm^2 ^{208}Pb target with a 187 MeV ^{12}C beam. The α-particle lower energy counter cutoff for these (and other) spectra is seen to be ~20 MeV. The prominent features of these spectra are the same as those reported by Britt and Quinton [1]. At forward angles the spectra are dominated by a broad, bell shaped peak centered a few MeV below the beam velocity.

The angular distribution of the energy-integrated differential cross section is shown in fig. 9. It is strongly peaked in the forward direction, increasing almost exponentially with decreasing

laboratory angle. As was determined previously [1], the evaporation α-particles show a relatively flat $d\sigma/d\Omega$ angular distribution. The total α-particle production cross section was obtained by integrating the angular distribution shown in fig. 9 from $0<\theta_\alpha<50°$. Extrapolation of this angular distribution to near zero degrees was done as indicated by the dashed line. For $E(^{12}C)=187$ MeV the total α-particle cross section was found to be ~1100 mb (±25%). This is quite similar to the α-particle production cross section measured by Wilczynska et al.[10]. For comparison, the geometric and total reaction cross sections are about 2200 and 3600 mb, respectively.

Particle-particle coincidence measurements were performed with vertically arranged ΔE-E type telescopes as described in section III. For the bombarding energies of 132 and 187 MeV, only the 1-2 detection system was employed. At the highest energy, 230 MeV, all three coincidence combinations were recorded. Figure 10a shows the summed energy of coincident events (corrected for randoms) in which one telescope recorded an α-particle and any particle entered the second telescope. Three features are prominent: two quasielastic peaks near the beam energy and a broad bump centered slightly below two-thirds of the beam energy. The peak at 178 MeV is determined kinematically to be the quasielastic breakup of ^{12}C into the α and ^{8}Be channel (Q-value = -7.28 MeV). This interpretation is based further on the observation that the particle identification spectrum in the other telescope, corresponding to events in this peak, shows a

single grouping near the ^{7}Li position, as is expected if two α-particles of approximately the same energy simultaneously entered this telescope (see section III). (An actual α+^{7}Li coincidence is ruled out by Q-value considerations.)

The second quasielastic peak corresponds to α+^{9}Be coincidences which result from the decay of excited ^{13}C nuclei that are produced via a neutron pickup to ^{13}C states located above the breakup threshold. This transition is discussed in more detail elsewhere [23].

Figure 10b shows the total energy spectrum when both telescopes register an α-particle in coincidence (it should be noted from this spectrum that the majority of coincident events in fig. 10a arise from such 2α coincidences). Most of the contribution to the fig. 10b spectrum arises from decaying ^{8}Be nuclei; as will be discussed below, however, there is some contribution from the sequential 3α decay of ^{12}C with only one α-particle from ^{8}Be being recorded in a given telescope.

Further interpretation of the character of the ^{12}C* breakup transition can be obtained from the ^{8}Be projected energy spectrum arising from α+^{8}Be(2α) events yielding a total energy of 178 MeV. Such a spectrum is shown in fig. 11. The nature of the contribution to this projected ^{8}Be spectrum from different breakup states of ^{12}C will depend upon the relative energy of the fragments, as well as upon the individual telescope collimator sizes and the angular separation between the telescopes. Thus the 0^{+}, 7.66 MeV state of ^{12}C (ref. 25)

will have a breakup energy of ε = 0.288 MeV which, with this detection geometry, results in a broad peak at ~120 MeV, while the 3^-, 9.64 MeV state, for which ε = 2.27 MeV, results in two narrow peaks. Evidence of higher excited states is not seen, either because of counter cut-off effects or because the state is broad, e.g., at 10.8 MeV.

The probabilities for detecting (with a two telescope system) quasielastic breakup events corresponding to the 7.6 and 9.6 MeV states of ^{12}C were calculated with a Monte Carlo simulation code. This numerical calculation assumed that all breakup fragments are distributed isotropically with respect to the $^{12}C^*$ rest frame. While this is true for the 0^+, 7.6 MeV state, it is an assumption for the 3^-, 9.6 MeV state and so will introduce a potential error whose magnitude is difficult to assess because of our lack of knowledge of the reaction mechanism and the transition probabilities. For instance, the Monte Carlo simulation showed that, if the 7.6 and 9.6 MeV ^{12}C states are equally populated, then the experimental contribution to the quasielastic peak in fig. 10a from the 7.6 MeV state should be a factor of 6.7 greater than the contribution from the 9.6 MeV state. However, the experimental value is 16:1. The difference between these two ratios could either indicate that the 7.6 MeV state has a higher excitation probability than the 9.6 MeV state or that the observed yield of the 3^-, 9.6 MeV state is suppressed due to spin alignment. (For certain extreme conditions of alignment the detection probability of $^{12}C^*$

(9.6 MeV) at this energy may be reduced by as much as a factor of seven). Similar arguments may be applied to higher states which were investigated with the other two detector configurations 2-3 and 1-3 at a ^{12}C bombarding energy of 230 MeV. Table 2 contains typical $^{12}C^*$ quasielastic breakup detection efficiencies for the three telescope combinations at the highest bombarding energy investigated.

The summed differential cross sections of the quasielastic peak (7.6 and 9.6 MeV ^{12}C states only) for the three energies investigated are shown in fig. 12a. Each angular distribution is found to peak near the grazing angle suggesting that this breakup process is a peripheral phenomenon. The total $^{12}C^*$ production cross section as measured with detector combination 1-2 was estimated by extrapolating the angular distributions to small angles and is shown in fig. 12b. Total cross sections are found to be of the order of millibarns, far below the total α-particle cross sections for these bombarding energies. Measurements at 230 MeV with the other telescope combinations 1-3 and 2-3 permit the conclusion that the production of $^{12}C^*$ nuclei with excitation energies between 9.6 and 16 MeV is also negligible, compared to the total α-particle cross section. An upper estimate of the maximum differential cross section at 230 MeV for $^{12}C^*$ production with excitation energies above 9.6 MeV is ~15 mb/sr. Thus the production of sequentially decaying ^{12}C nuclei is not a significant source of fast alpha particles.

The observation of a total quasielastic $^{12}C^*$ production cross section of the order of a few millibarns is consistent with inelastic scattering studies with a ^{12}C target (cf. ref. 26-28). Analysis of $\alpha+^8Be$ coincidences for more negative Q-values (a mutual excitation process which could be confused with $\alpha-^7Li$ events) does not alter the conclusion that $^{12}C^*$ production and subsequent sequential decay is not a prominent source of fast alpha particles. The specific analysis of this quasielastic channel in terms of folded potentials and the D.W.B.A. is presented elsewhere[29].

Figure 13a shows a $(^{12}C,\alpha\alpha)$ spectrum taken with detector system 1-2. Figures 13b-13e show projected α energy spectra for $\alpha+\alpha$ events with a total energy located within the indicated gates. The prominent peak centered at one-half of the total $\alpha+\alpha$ energy is kinematically consistent with the production of ^8Be(g.s.) nuclei (decay energy of .092 MeV, ref. 30). The broad, weak bumps are consistent kinematically with the decay of the broad 2.94 MeV, first excited state of ^8Be. For this detector configuration the probability of detecting ^8Be(g.s.) nuclei was a factor of 5-10 larger than that of detecting ^8Be(2.94 MeV) nuclei.

Further confirmation that mainly ^8Be nuclei were detected, rather than uncorrelated 2α production, comes from fig. 14 which shows a $(^{12}C,\alpha\alpha)$ spectrum taken with the 2-3 detector system. This system has a telescope-to-telescope angular separation greater than the ^8Be(g.s.) decay cone, but

not that of the ^{8}Be(2.94 MeV) decay cone. Thus, as is discussed below, if ^{8}Be(2.94 MeV) is produced in the reaction, we expect to see the observed double bump structure in the projected spectra, reflecting sequential decays from the broad first excited state of ^{8}Be.

The Monte Carlo program to calculate detection probabilities can also predict the spectral shape of such projected spectra. Figure 15 presents the predicted ^{8}Be(2.94 MeV) projected energy spectra for the three detector configurations used in this work. Since the first excited state of ^{8}Be is broad, a continuous Lorentzian distribution of width equal to 1.56 MeV was used to specify the decay energy. Two prominent features emerge in fig. 15: 1) the projected spectra of the two closest configured telescope pairs exhibit a double peaking and 2) the two peaks in figs. 15a and 15b merge into a continuous (resembling almost a three-body phase space) distribution as the separation angle is increased, as shown in fig. 15c. The double peaking in the projected energy spectra is a simple consequence of the sequential decay kinematics and the detector configuration. It is seen that fig. 15b resembles fairly closely the projected energy spectrum from gate 1 of fig. 14. Hence, it can again be concluded that both ^{8}Be(g.s.) and ^{8}Be(2.94 MeV) nuclei are produced in these $^{12}C+^{208}Pb$ reactions.

Figure 16 shows a $^{12}C(^{12}C,\alpha\alpha)$ total energy spectrum at 230 MeV bombarding energy for comparison with fig. 14a. The shape is rather similar to that obtained with the ^{208}Pb target

except that the broad, bell-shaped peak is centered at significantly lower energies than that obtained with the heavy target.

Figures 17, 18 and 19 show Wilczynski-type diagrams for ^{8}Be(g.s.) production at the three bombarding energies investigated. These diagrams plot contours of the double differential cross section $d^2\sigma/d\Omega dE$ for the ^{8}Be(g.s.) reaction products as a function of their kinetic energy and their laboratory scattering angle. Such diagrams highlight both the energy and the angular distributions. All three figures show a ridge near beam velocity which extends from the maximum towards backward angles. There is little or no evidence of a ridge extending back from zero degrees as is characteristic of a deep inelastic reaction. The ridge is therefore likely to be associated with an interaction which is peripheral in nature. No other significant features are evident.

Figure 20 shows the absolute differential cross section for the production of ^{8}Be(g.s.) nuclei. These cross sections were obtained by integrating the (^{12}C,$\alpha\alpha$) spectra by energy bins with the appropriate detection probability for ^{8}Be(g.s.) nuclei folded in. A similar procedure was performed for the ^{8}Be(2.94 MeV) events (for which the angular distributions are not shown). Detection probability is discussed in Section III. The angular distributions of both ^{8}Be products are very similar. Increasing cross section with decreasing angles and steeper angular distributions with increasing bombarding energy are evident in

fig. 20. Cross sections up to several hundred millibarns are apparent, suggesting that a significant fraction of the inclusive α-particles arise from decaying ^{8}Be nuclei.

Further information can be obtained from the shapes of these angular distributions. The shift in the angle of the peak of each angular distribution suggests that there is an interaction radius, R_i, such that outside R_i the ^{8}Be production cross section decreases with increasing radius and inside R_i the ^{8}Be nuclei are absorbed to a high extent. In cases where the Sommerfeld parameter $\eta >> 1$, it is possible to try to correlate the emission angle θ with the distance of closest approach, R_{min}. If it is assumed that the ^{8}Be nuclei continue approximately on the Rutherford trajectory of the incoming ^{12}C projectile, then the following relation exists between R_{min} and θ, the center-of-mass scattering angle:

$$R_{min} = \frac{Z_p Z_T e^2 \ (1+1/\sin(\theta/2))}{2E_{cm}} \quad . \qquad (1)$$

Using equation (1) it is possible to transform the angular distribution $d\sigma/d\Omega$ into the quantity $d\sigma/R_{min}dR_{min}$ via the expression:

$$\frac{d\sigma}{dR_{min}} = \frac{-16\pi E_{cm}}{Z_p Z_T e^2} \sin^3 (\theta/2) \frac{d\sigma}{d\Omega} \quad . \qquad (2)$$

Angular distributions from heavy-ion collisions have been analyzed previously in this manner [1,31,32].

Figure 21 shows the experimental angular distribution of ^{8}Be(g.s.) nuclei transformed into $d\sigma/R_{min}dR_{min}$. The quantity $d\sigma/R_{min}dR_{min}$ can be interpreted as a measure of the probability of ^{8}Be production at a given distance of closest approach. (Due to distortion by the nuclear potential this view should be taken cautiously). In this representation the form of the angular distribution should be approximately independent of the beam energy. It is seen that the distributions peak near 12 fermis, which corresponds very closely to the sum of the radii for the target and projectile for an r_0 = 1.5 fm. Grazing collisions are most probable; interactions which produce ^{8}Be at other radii are hindered.

For a direct comparison of singles α-particles and ^{8}Be cross sections, the integrated total cross sections for ^{8}Be(g.s.) production are shown in fig. 22. ^{8}Be(2.94 MeV) production cross sections also were obtained for two bombarding energies $E(^{12}C)$ = 187, 230 MeV; the detection efficiency of ^{8}Be(2.94) nuclei for the 132 MeV bombarding energy was too low for its observation. Total cross sections for ^{8}Be(2.94 MeV) production were found to be 175 mb and 180 mb at 187 and 230 MeV, respectively. The ratios of the production of ^{8}Be(g.s.) to ^{8}Be(2.94 MeV) are 1:1.9 and 1:1.85 for the 187 and 230 MeV bombarding energies, respectively. Figure 22 indicates a rapid rise in the ^{8}Be g.s. cross section over the energy range of 12-16 MeV/A. This trend

is consistent with the rapid rise in α-particle production cross sections measured between 90 and 200 MeV ^{12}C bombarding energy.[10] Furthermore, total ^{8}Be cross sections, by virtue of their magnitude, are clearly able to explain a significant portion of the inclusive α-particles.

From the measurements of Siwek-Wilczynska et al. [10] it is known that ~20-40% of the inclusive α-particles result from the incomplete fusion reactions ($^{12}C,\alpha$) and ($^{12}C,2\alpha$). The combined ^{8}Be measurements reported here for the g.s. and first excited state are far in excess of the ($^{12}C,2\alpha$) cross sections for incomplete fusion, see fig. 2b. Hence, projectile fragmentation must be responsible. It can be concluded that for each ^{8}Be observed in excess of the incomplete fusion 2α's expected, a third α-particle was liberated initially. Therefore, a numerical accounting of the origin of inclusive α-particles for $E(^{12}C)$ = 187 MeV can be obtained with the following assumptions: i) 20-40% of the inclusive α-particles result from the incomplete fusion process [10]; ii) the incomplete fusion reactions ($^{12}C,\alpha$) and ($^{12}C,2\alpha$) have about the same cross section [10]; and iii) the ^{8}Be's that do not originate in an incomplete fusion process are accompanied by a third α-particle. Given these assumptions, some 80-90% of the inclusive α-particles can be accounted for. Furthermore, it can be concluded that at the bombarding energy of 187 MeV, projectile fragmentation into $\alpha+^{8}Be$ particles without absorption is the largest source of α-particles.

The excitation function for α-particle production between 90 and 200 MeV ^{12}C bombarding energy shows a steep rise toward larger α-particle total cross sections at higher energies[10]. If this trend continues above 200 MeV beam energy, the measured ^{8}Be (g.s., 2.94 MeV) cross sections at 230 MeV bombarding energy will explain a smaller fraction of the inclusive α-particles. (A partial angular distribution of singles α-particles for the 230 MeV beam indicates that the cross section may not increase as rapidly above this 90-200 MeV interval, but it is increasing slightly faster than the rise in the production of ^{8}Be). It is concluded that other breakup channels such as direct three α-particle production or additional fragmentation processes contribute more cross section at the higher energies.

Of the ^{8}Be nuclei observed, the ratio between ^{8}Be(g.s.) and ^{8}Be(2.94 MeV) production is the same for the two higher bombarding energies (187 and 230 MeV) for which data are available. This strongly suggests that projectile ground state properties are important in the projectile fragmentation process(es). In addition, the observed large production of ^{8}Be(2.94 MeV) nuclei is consistent with the suggestion from measurements of 126 MeV ^{12}C on ^{197}Au [15] that a significant fraction of the ^{8}Be nuclei was being produced in an excited state. As is well known, pickup reactions and cluster model calculations (ref. 25 and references therein, ref. 33) indicate a substantial amplitude for representing a ^{12}C nucleus not only as $[\psi(^{8}Be(g.s.)) \times \psi(\alpha)]$ but also with the configurations

$[\psi(^{8}Be(2.94\ MeV)) \times \psi(\alpha)]$ and $[\psi(^{8}Be(11.4,\ 4^{+})) \times \psi(\alpha)]$. Transitions through the 11.4 MeV ^{8}Be state apparently are not important at the bombarding energy of 187 MeV. (Verification of ^{8}Be(11.4 MeV) production would be difficult owing to the large decay energy and therefore the tendency for the sequential decays to appear as uncorrelated 2α-particle production.)

In fig. 22, the observed increasing trend of ^{8}Be g.s. production as a function of bombarding energy at first appears inconsistent with the predictions of the incomplete fusion sum rule model (see fig. 2b. and discussion in section II). Qualitatively, a large multibody fragmentation channel should become more prominent as the bombarding energy increases. The ^{8}Be measurements reported are specifically for a weakly bound fragment. As the bombarding energy is increased it is quite conceivable that the projectile-target interaction, which leads to fragmentation, becomes more "severe". This in turn, would suggest a decrease in probability for the rather weakly bound ^{8}Be nuclei to survive the breakup process. An extension of these measurements of the production of the resonant nucleus ^{8}Be in conjunction with inclusive α-particle cross section measurements at higher ^{12}C bombarding energies could elucidate this point further.

V. Summary and Conclusion

The mechanisms involved in the production of fast α-particles in a ^{12}C induced reaction on a ^{208}Pb target

have been investigated at the bombarding energies of 132, 187 and 230 MeV. With double and triple coincidence measurements, absolute cross sections have been determined for the reactions (^{12}C,^{8}Be(g.s.)), (^{12}C,^{8}Be(2.94 MeV)) and (^{12}C,$^{12}C^{*}_{\rightarrow\alpha+^{8}Be}$). It was determined that the simple inelastic scattering process (^{12}C,$^{12}C^{*}_{\rightarrow\alpha+^{8}Be}$) observed from 13 to 41 degrees does not contribute significantly to the large production of fast α-particles (~950 mb over the same angular range). However, the observation of a large production cross section for ^{8}Be(g.s.) and ^{8}Be(2.94 MeV) nuclei at E(^{12}C) = 187 MeV permitted the conclusion that, as first suggested by Britt and Quinton[1], projectile fragmentation is largely responsible for the fast α-particle production.

The measurements reported here, together with those of Siwek-Wilczynska et al [9,10] provide an explanation for the origin of over 80% of the observed α-particles at 187 MeV bombarding energy. Although the observed ^{8}Be production cross sections as a function of the bombarding energy are not in disagreement with the simple incomplete fusion model predictions of Siwek-Wilczynska et al., it is clear that projectile spectroscopic and/or final state interactions are important in fragmentation reactions at these bombarding energies. It is concluded that an angular correlation measurement of $\alpha+^{8}Be$ reaction products would be feasible and very valuable to a further understanding of the breakup mechanism(s) involved.

The results presented here suggest several interesting experiments, some complementary to this work and some of a more general nature. A detailed study of the production cross section of ^{8}Be from ^{10}B, ^{13}C, ^{14}N, ^{16}O and ^{20}Ne induced reactions would prove interesting, as would a more detailed comparison between the cluster configurations in the various projectiles and the fragmentation channels which are observed to be strong. Of spectroscopic interest, a comparison between the (^{9}Be,^{8}Be(g.s.)) reaction (cf. ref. 34) and the unstudied, but definitely feasible, (^{9}Be,^{8}Be(2.94 MeV)) reaction could yield helpful spectroscopic information.

‡This work was supported by the Director, Office of Energy Research, Office of High Energy and Nuclear Physics of the U.S. Department of Energy under contract No. DE-AC03-76SF00098. The authors would also like to thank Dr. D. P. Stahel for his assistance during the early phase of this work.

Figure Captions

Fig. 1. Semiclassical calculation of the maximum transferred angular momentum to the residual target nucleus versus the transferred fragment mass. The dashed line represents the critical angular momentum calculated from the balance of forces.

Fig. 2. a) Calculation of the incomplete fusion sum rule model probability factors for various reaction channels as a function of angular momentum for the $^{12}C+^{208}Pb$ system. (See text). b) Excitation functions as predicted by the incomplete fusion sum rule model. (See text).

Fig. 3. Schematic diagram of the triple telescope system employed for coincidence measurements.

Fig. 4. The percentage efficiency of detecting ^{8}Be(g.s.) versus its total kinetic energy. The effective solid angle is the solid angle of the two counter system multiplied by the detection efficiency. The two telescopes were assumed to have a vertical center-to-center angular separation of 5.9°. Counter cutoffs are determined by the operating region of the telescopes for the detection of α particles.

Fig. 5. Same as fig. 4 except ^{8}Be(2.94 MeV) decays were assumed.

Fig. 6. Similar to fig. 4 except that the detection of three alpha particles from the decay of the $^{12}C^{*}$ (7.6 MeV) state in the two particle telescopes is assumed. The solid

curve is for any two α-particles to enter one telescope and the third α-particle in the other telescope. The dashed line is the calculation which required the two α's from the ^{8}Be to enter a single counter. Lower and upper energy cutoffs for an α-particle were 19 and 124 MeV, respectively.

Fig. 7. Similar to fig. 6 except the detection of the $^{12}C^{*}$ (9.6 MeV) state is assumed.

Fig. 8. Alpha-particle inclusive spectra at four laboratory angles for the reaction of 187 MeV ^{12}C ions incident on ^{208}Pb.

Fig. 9. Angular distribution of the measured inclusive α-particles for the $^{12}C+^{208}Pb$ system at 187 MeV bombarding energy.

Fig. 10. a) The yield of coincident events between the two telescopes from the reaction of 187 MeV ^{12}C on ^{208}Pb with the requirement that one telescope record an α-particle, plotted as a function of the summmed energy in the two telescopes. b) As for a), but with the requirement that both telescopes simultaneously record an α-particle.

Fig. 11. The energy of ^{8}Be nuclei in coincidence with an α-particle for the transition $^{208}Pb(^{12}C,\alpha^{8}Be)$ $^{208}Pb(g.s.)$ at 187 MeV bombarding energy. This projected energy spectrum was taken at $\theta_{lab}=19°$ with the detector configuration which has an average vertical angular separation of $\Delta\phi=5.9$.

Fig. 12. a) Angular distributions for the quasielastic production of $^{12}C^*$ (7.6 MeV) and $^{12}C^*$ (9.6 MeV) at three bombarding energies. b) The summed cross section for the angular distributions in a).

Fig. 13. a) Summed energy spectrum for the reaction $^{208}Pb(^{12}C,\alpha\alpha)$ at a ^{12}C bombarding energy of 187 MeV. The average vertical angular separation of the two particle telescopes was $\Delta\phi=5.9°$. b)-e) Projected α energy spectra for total $\alpha_1+\alpha_2$ energies falling within the gates indicated in a).

Fig. 14. Summed energy spectrum for the reaction $^{208}Pb(^{12}C,\alpha\alpha)$ at a ^{12}C bombarding energy of 230 MeV and a detector system location of $\theta_{lab}=14°$. The average vertical angular separation of the two particle telescopes was $\Delta\phi=10.9°$. Projected α energy spectra are beneath the total energy spectrum. The projected spectra correspond to the energy gates indicated.

Fig. 15. Monte Carlo simulation of the expected projected energy spectra of $\alpha+\alpha$ coincidences which arise from the decay of ^{8}Be (2.94 MeV) for three detector configurations. An ejectile kinetic energy of 150 MeV was assumed. Parts a), b) and c) indicate the different center-to-center telescope separations, $\Delta\phi$.

Fig. 16. Summed energy spectrum for the reaction $^{12}C(^{12}C,\alpha\alpha)$ at a ^{12}C bombarding energy of 230 MeV and a detector system location of $\theta_{lab}=14.5°$. The average vertical angular separation of the two particle telescopes was $\Delta\phi=5.9°$.

Fig. 17. Wilczynski-type diagram for the production of ^{8}Be(g.s.) nuclei for the system 132 MeV $^{12}C+^{208}Pb$. The solid curves indicate contours of constant cross section.

Fig. 18. Wilczynski-type diagram for the production of ^{8}Be(g.s.) nuclei for the system 187 MeV $^{12}C+^{208}Pb$.

Fig. 19. Wilczynski-type diagram for the production of ^{8}Be(g.s.) nuclei for the system 230 MeV $^{12}C+^{208}Pb$.

Fig. 20. Angular distributions for the production of ^{8}Be(g.s.) nuclei for the system $^{12}C+^{208}Pb$ at three ^{12}C bombarding energies: 132, 187 and 230 MeV.

Fig. 21. The production probability of ^{8}Be(g.s.) nuclei versus the distance of closest approach, R_{min}, for the $^{12}C+^{208}Pb$ system at three bombarding energies: 132, 187, and 230 MeV.

Fig. 22. The total production cross section of ^{8}Be(g.s.) nuclei for the $^{12}C+^{208}Pb$ system at three bombarding energies: 132, 187 and 230 MeV.

Table Captions

1. Detection system geometry for the three, particle-telescope systems. Refer to fig. 3 for the telescope numbering scheme.

2. Detection efficiency of $\alpha+2\alpha$ events resulting from the sequential decay of $^{12}C^*$ for a total kinetic energy of 221 MeV. Dashes indicate transitions which are expected to be weak. See also fig. 3.

References

1) H. C. Britt and A. R. Quinton, Phys. Rev. 124 (1961) 877.

2) J. Galin, B. Gatty, D. Guerreau, C. Rousset, U. C. Schlotthauer-Voos and X. Tarrago, Phys. Rev. C9 (1974) 1126.

3) T. Inamura, M. Ishihara, T. Fukuda, T. Shimoda and H. Hiruta, Phys. Lett. 68B (1977) 51.

4) H. Yamada, D. R. Zolnowski, S. E. Cala, A. C. Kahler, J. Pierce and T. T. Sugihara, Phys. Rev. Lett. 43 (1979) 605.

5) C. M. Castaneda, H. A. Smith, T. E. Ward and T. R. Nees, Phys. Rev. C16 (1977) 1437.

6) C. M. Castaneda, H. A. Smith, P. P. Singh, J. Jastrzebski, H. Karwowski and A. K. Gaigalas, Phys. Lett. 77B (1978) 371.

7) D. R. Zolnowski, H. Yamada, S. E. Cala, A. C. Kahler and T. T. Sugihara, Phys. Rev. Lett. 41 (1978) 92.

8) K. A. Geoffroy, D. G. Sarantites, M. L. Halbert, D. C. Hensley, R. A. Dayras and J. H. Barker, Phys. Rev. Lett. 43 (1979) 1303.

9) K. Siwek-Wilczynska, E. H. du Marchie van Voorthuysen, J. van Popta, R. H. Siemssen and J. Wilczynski, Phys. Rev. Lett. 42 (1979) 1599.

10) K. Siwek-Wilczynska, E. H. du Marchie van Voorthuysen, J. van Popta, R. H. Siemssen and J. Wilczynski, Nucl. Phys. A330 (1979) 150.

11) J. H. Barker, J. R. Beene, M. L. Halbert, D. C. Hensley, M. Jääskeläinen, D. G. Sarantites and R. Woodward, Phys. Rev. Lett. 45 (1980) 424.

12) J. Wilczynski, K. Siwek-Wilczynska, J. Van Driel, S. Gonggrijp, D. C. J. M. Hageman, R. V. F. Janssens, J. Lukasiak and R. H. Siemssen, Phys. Rev. Lett. 45 (1980) 606.

13) C.C. Hsu, D. J. Morrissey, L. W. Richardson, G. J. Wozniak and L. G. Moretto, LBL preprint LBL-12519 (1981), to be published.

14) Y. Eyal, K. Beg, D. Logan, J. Miller and A. Zebelman, Phys. Rev. C8 (1973) 1109.

15) R. L. Kozub, D. Logan, J. M. Miller and A. M. Zebelman, Phys. Rev. C10 (1974) 1246.

16) J. B. Ball, C. B. Fulmer, M. L. Mallory and R. L. Robinson, Phys. Rev. Lett. 40 (1978) 1698.

17) B. G. Harvey, Notas de Fisica 3, No. 1 (1980) 99.

18) D. M. Brink, Phys. Lett. 40B (1972) 37.

19) J. Wilczynski, Nucl. Phys. A216 (1973) 386.

20) A. G. Artukh, V. V. Avdeichikov, J. Erö, G. F. Gridnev, V. L. Mikheev, V. V. Volkov and J. Wilczynski, Nucl. Phys. A160 (1971) 511.

21) V.V. Volkov, Sov. J. Part. Nucl. 6, No. 4 (1976) 420.

22) G. J. Wozniak, H. L. Harney, K. H. Wilcox and J. Cerny, Phys. Rev. Lett. 28 (1972) 1278.

23) A. N. Bice, Ph.D. Thesis, University of California, Berkeley, (January, 1982) LBL report, LBL-13859.

24) A. C. Shotter, A. N. Bice, D. P. Stahel and J. Cerny, J. Phys. G. 8 (1982) 355.

25) F. Ajzenberg-Selove, Nucl. Phys. A248 (1975) 1.

26) J. Specht, H. Rebel, G. Schatz, G. W. Schweimer, G. Hauser and R. Löhken, Nucl. Phys. A143 (1970) 373.

27) S. M. Smith, G. Tibell, A. A. Cowley, D. A. Goldberg, H. G. Pugh, W. Reichart and N. S. Wall, Nucl. Phys. A207 (1973) 273.

28) R. K. Bindal, K. Nagatani, M. J. Schneider, and P. D. Bond, Phys. Rev. C9 (1974) 2154.

29) R. Shyam, M. A. Nagarajan, A. C. Shotter, A. N. Bice, and J. Cerny, to be published.

30) F. Ajzenberg-Selove, Nucl. Phys. A320 (1979) 1.

31) J. A. McIntyre, T. L. Watts and F. C. Jobes, Phys. Rev. 119 (1960) 1331.

32) B. Neumann, H. Rebel, J. Buschmann, H. J. Gils, H. Klewe-Nebenius and S. Zagromski, Z. Phys. A296 (1980) 113.

33) D. Kurath, Phys. Rev. C7 (1973) 1390.

34) D. P. Stahel, G. J. Wozniak, M. S. Zisman, B. D. Jeltema and J. Cerny, Phys. Rev. C16 (1977) 1456.

Table 1. The Detection System Geometry

Telescope	Collimator Distance[a] Out-of-Plane: Upper Limit (cm.)	Lower Limit (cm.)	Radial Distance: Target to Telescope Center (cm.)	Angular Separation: Center-to-Center (deg.) Tel.1	Tel.2	Tel.3
1	-0.175	-1.0	11.52	---	5.9	16.8
2	1.0	0.175	11.52	5.9	---	10.9
3	3.19	2.49	11.85	16.8	10.9	---

a) The collimator width for all telescopes was 0.6 cm.

Table 2. The Percentage Efficiency of $^{12}C^*$ Detection

[E(^{12}C) Beam = 230 MeV]

$E_x(^{12}C)$ MeV	Telescopes 1-2 a.	Telescopes 1-2 b.	System Telescopes 1-3 a.	System Telescopes 1-3 b.	Telescopes 2-3 a.	Telescopes 2-3 b.
7.66	.820	---	0.	---	0.	---
9.64	.199	---	0.	---	.221	---
10.8	.127	---	.045	---	.084	---
11.83	---	.020	---	.015	---	.015
12.17	---	.011	---	.007	---	.010
14.08	---	.007	---	.006	---	.005
16.11	---	.004	---	.003	---	.003

a. α + ^{8}Be (g.s.) detection.

b. α + ^{8}Be (2.94 MeV) detection.

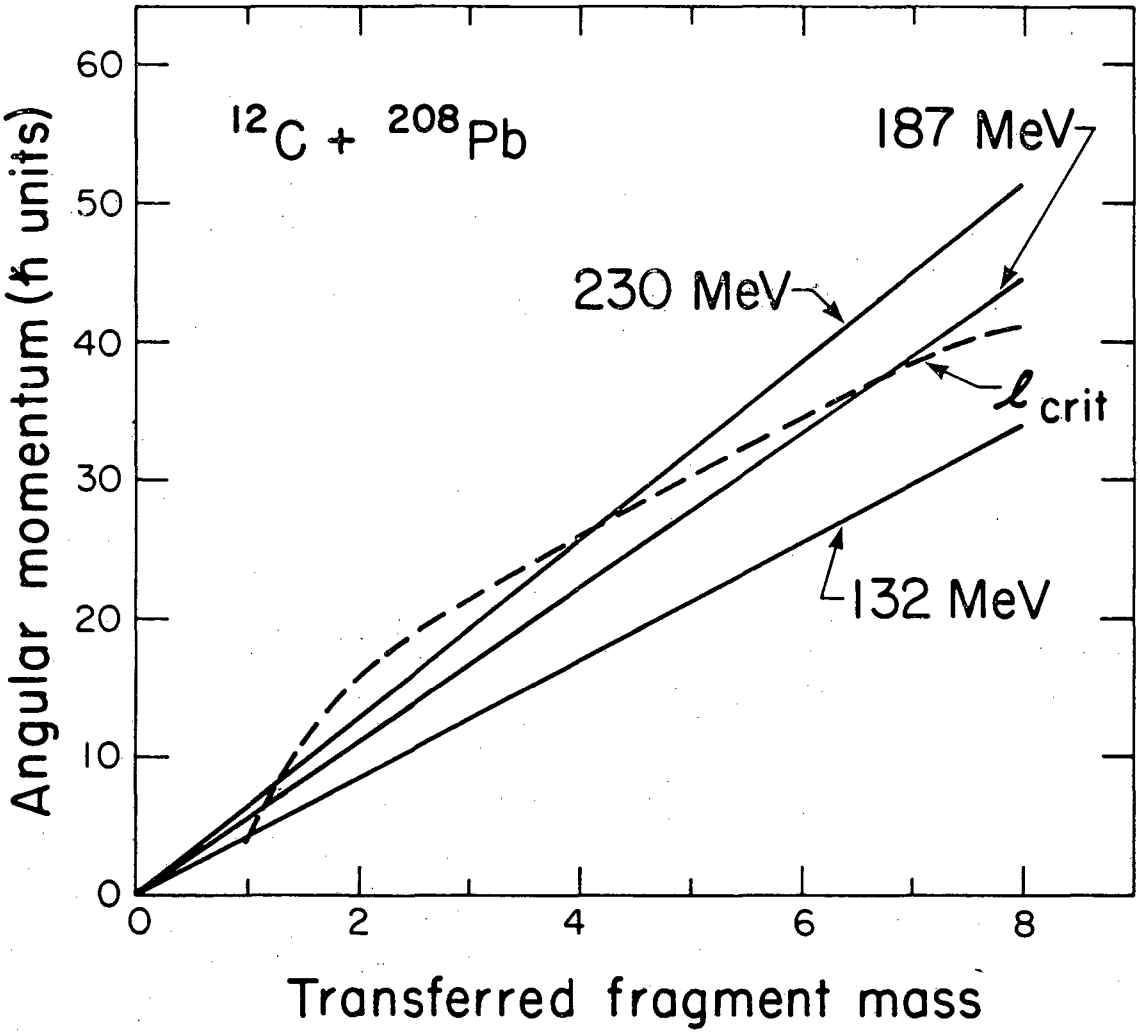

XBL8110-12001

Fig. 1

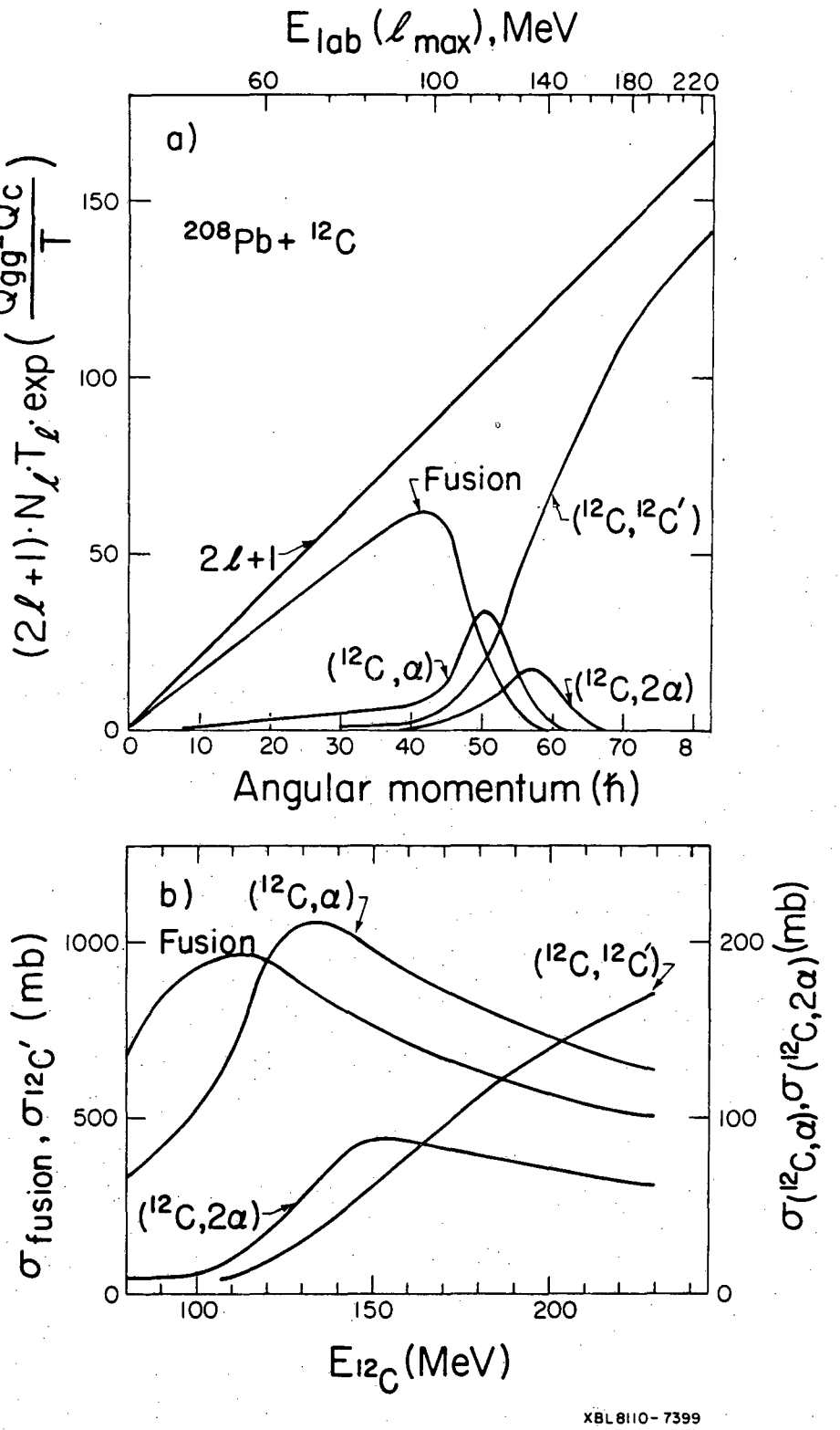
E lab (ℓ max), MeV
60
100
140
180
220
a)
208Pb+ 12C
(2ℓ+1)·N_ℓ·T_ℓ·exp((Qgg-Qc)/T)
150
100
50
0
Fusion
2ℓ+1
(12C,12C')
(12C,α)
(12C,2α)
0
10
20
30
40
50
60
70
8
Angular momentum (ħ)
b)
(12C,α)
Fusion
(12C,12C')
(12C,2α)
σfusion, σ12C' (mb)
1000
500
0
200
100
0
σ(12C,α), σ(12C,2α) (mb)
100
150
200
E12C (MeV)
XBL8110-7399

Fig. 2

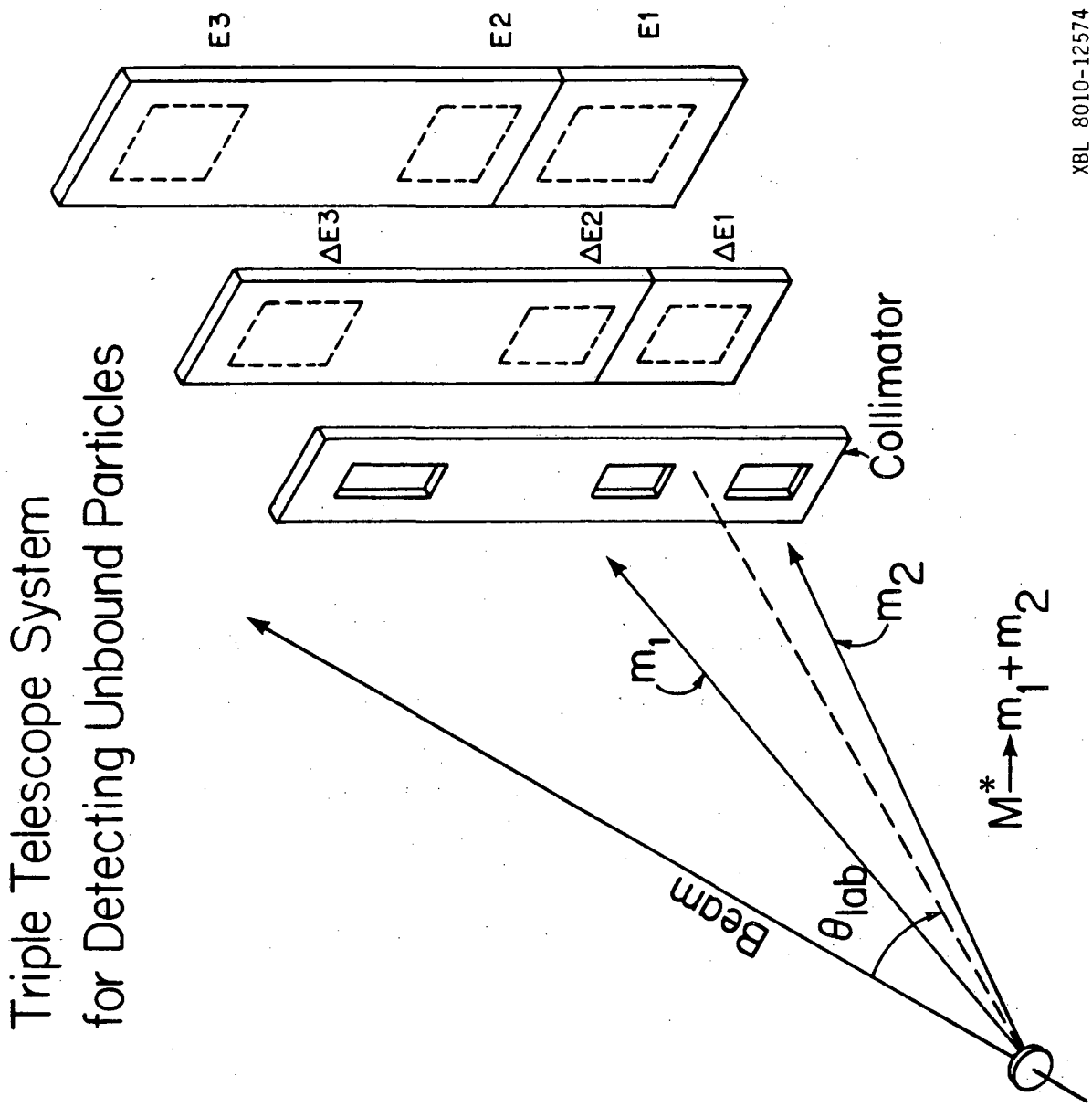
Triple Telescope System
for Detecting Unbound Particles
E3
E2
E1
ΔE3
ΔE2
ΔE1
Collimator
m_1
m_2
$M^* \rightarrow m_1 + m_2$
Beam
θ_{lab}
XBL 8010-12574

Fig. 3

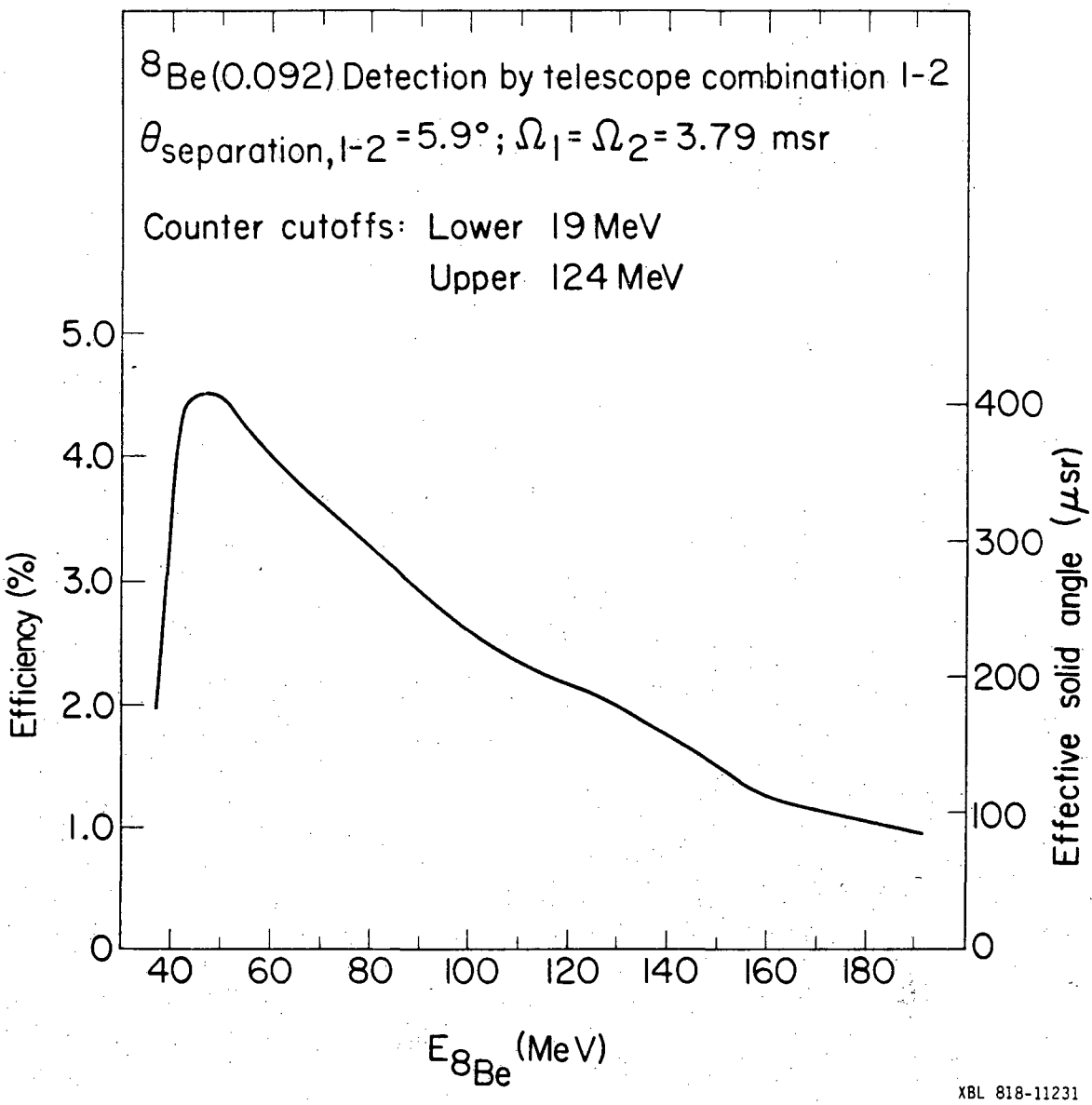
^{8}Be(0.092) Detection by telescope combination 1-2
$\theta_{separation,1-2} = 5.9°$; $\Omega_1 = \Omega_2 = 3.79$ msr
Counter cutoffs: Lower 19 MeV
Upper 124 MeV
Efficiency (%)
Effective solid angle (μsr)
$E_{^{8}Be}$ (MeV)
0
1.0
2.0
3.0
4.0
5.0
100
200
300
400
40
60
80
100
120
140
160
180
XBL 818-11231

Fig. 4

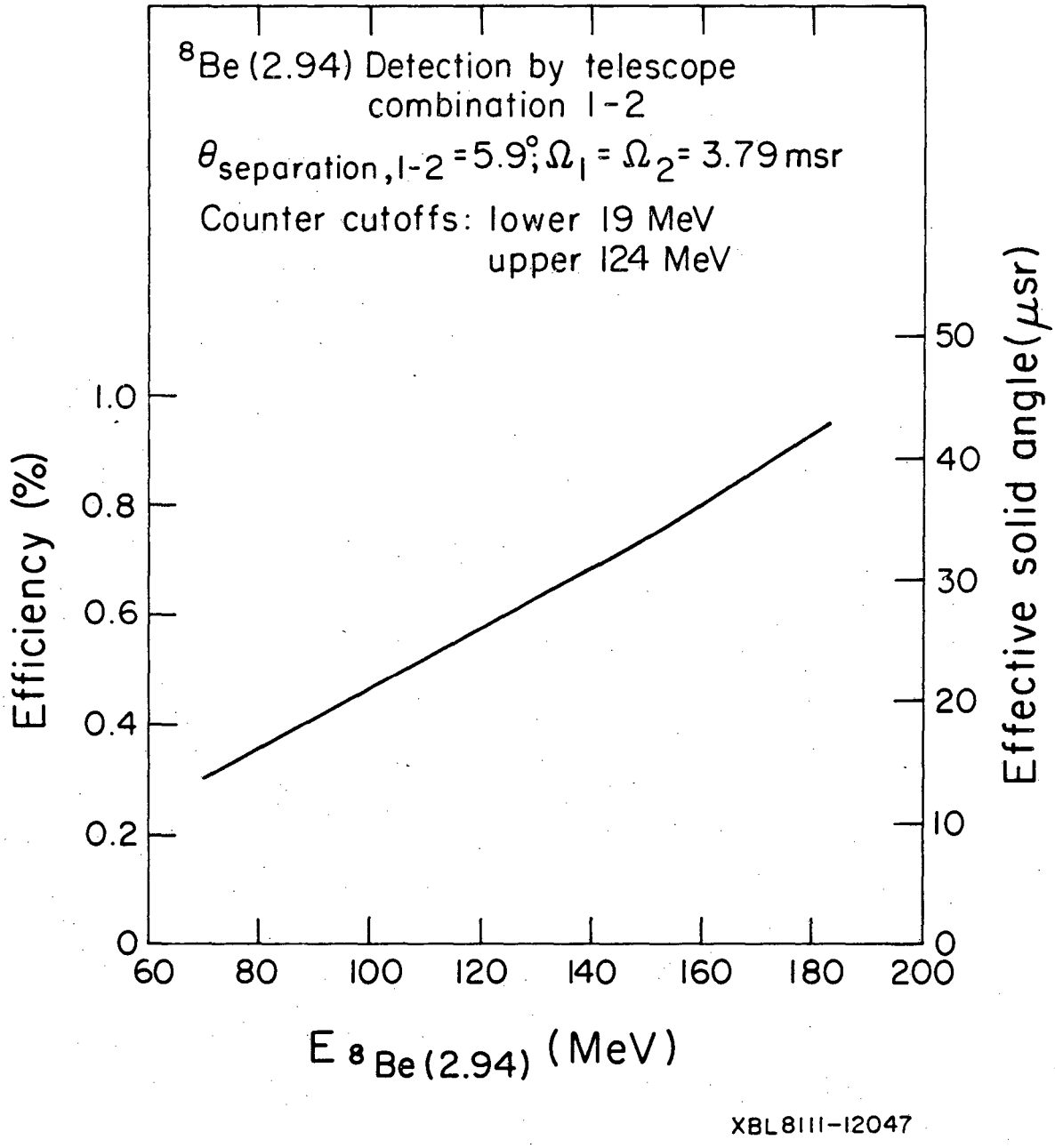
^{8}Be (2.94) Detection by telescope combination 1-2
$\theta_{separation,1-2} = 5.9°; \Omega_1 = \Omega_2 = 3.79$ msr
Counter cutoffs: lower 19 MeV
upper 124 MeV
Efficiency (%)
0
0.2
0.4
0.6
0.8
1.0
Effective solid angle (μsr)
0
10
20
30
40
50
60
80
100
120
140
160
180
200
$E_{^{8}Be(2.94)}$ (MeV)
XBL8111-12047

Fig. 5

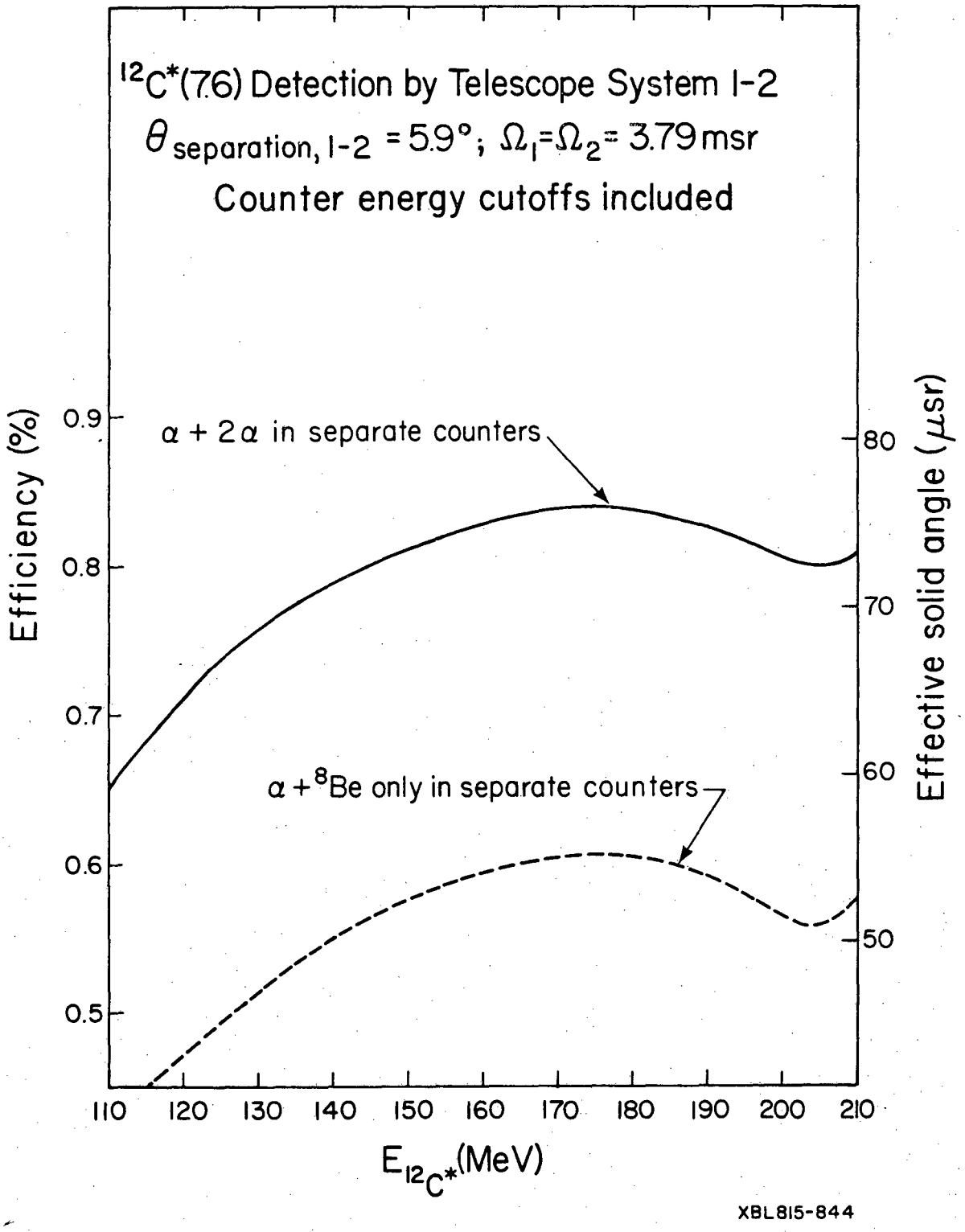
$^{12}C^*(7.6)$ Detection by Telescope System 1-2
$\theta_{separation,\ 1\text{-}2} = 5.9°$; $\Omega_1 = \Omega_2 = 3.79$ msr
Counter energy cutoffs included
$\alpha + 2\alpha$ in separate counters
$\alpha + {}^8Be$ only in separate counters
Efficiency (%)
0.9
0.8
0.7
0.6
0.5
Effective solid angle (μsr)
80
70
60
50
110
120
130
140
150
160
170
180
190
200
210
$E_{^{12}C^*}$(MeV)
XBL815-844

Fig. 6

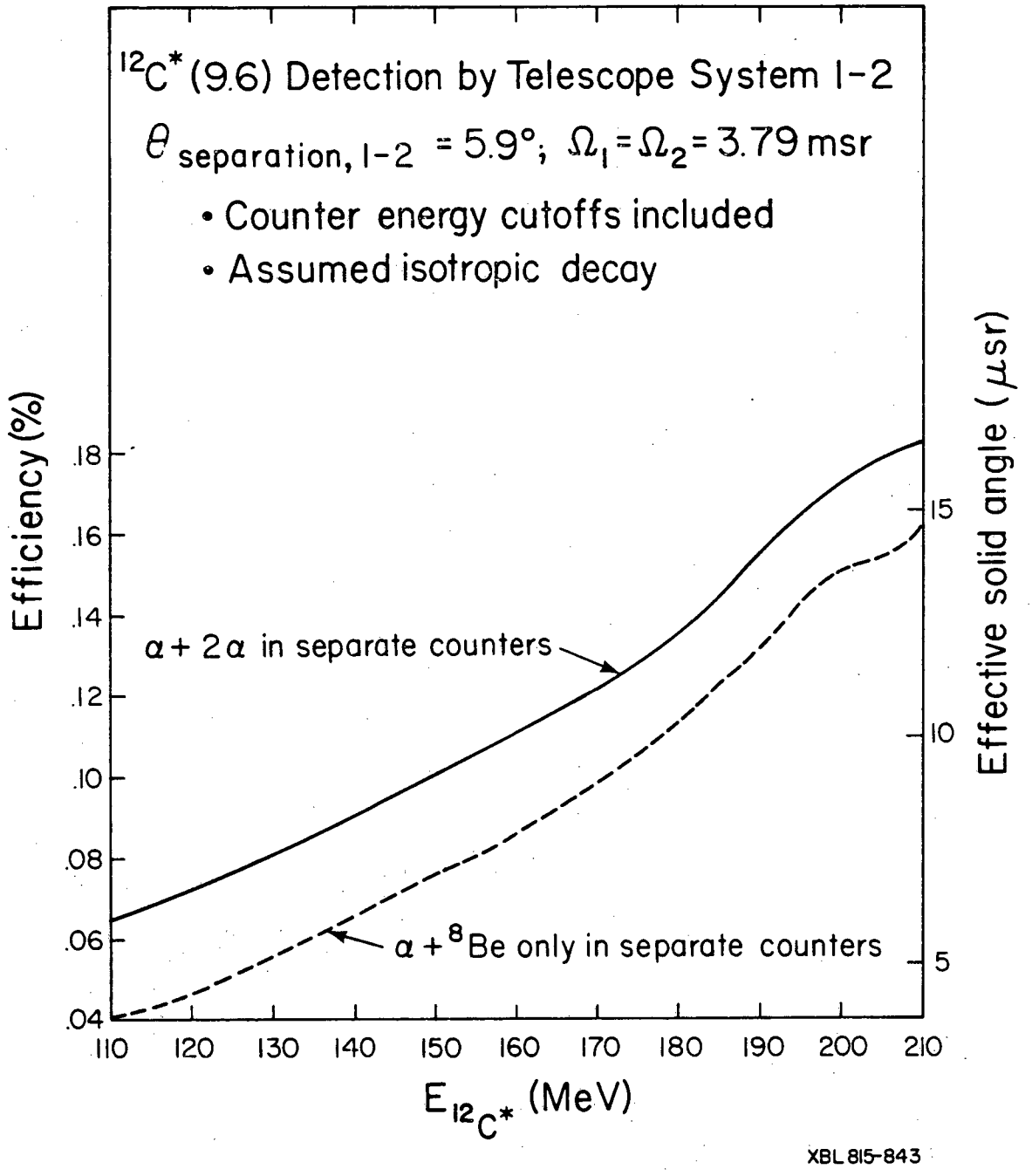
$^{12}C^*$(9.6) Detection by Telescope System 1-2
$\theta_{separation,\,1-2} = 5.9°$; $\Omega_1 = \Omega_2 = 3.79$ msr
• Counter energy cutoffs included
• Assumed isotropic decay
Efficiency (%)
.18
.16
.14
.12
.10
.08
.06
.04
α + 2α in separate counters
α + ^{8}Be only in separate counters
15
10
5
Effective solid angle (μsr)
110
120
130
140
150
160
170
180
190
200
210
$E_{^{12}C^*}$ (MeV)
XBL 815-843

Fig. 7

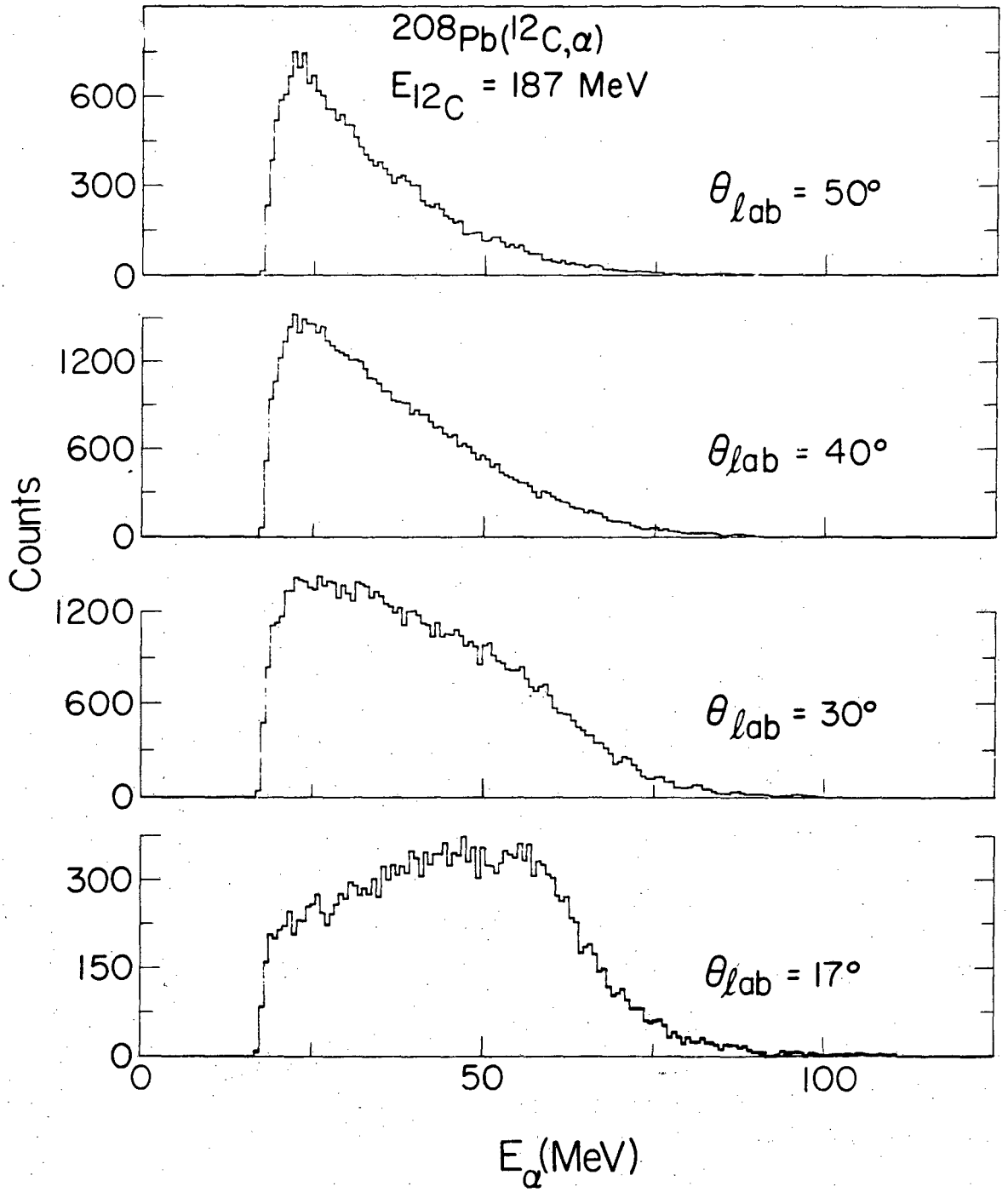

XBL 818-1166

Fig. 8

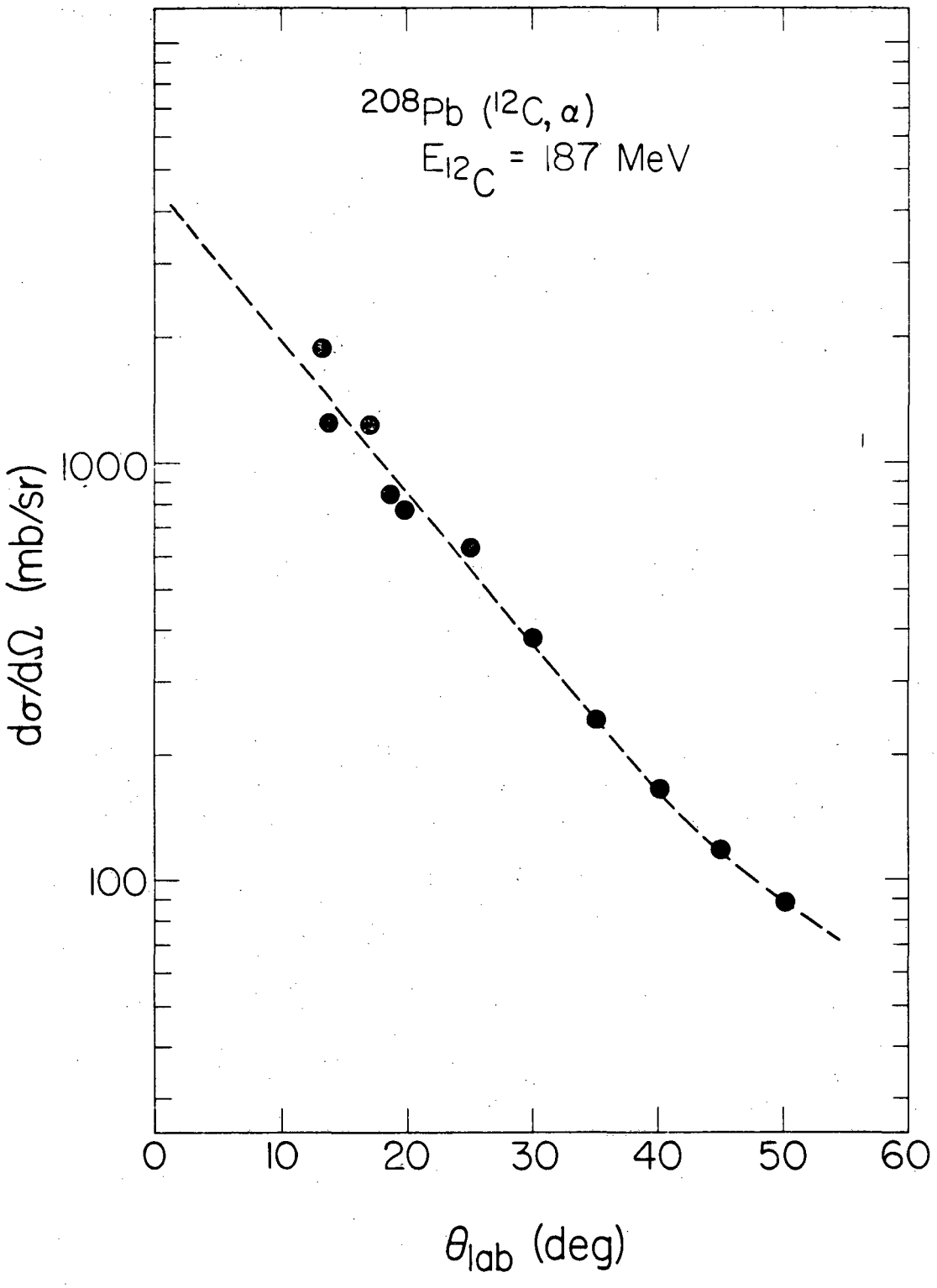
^{208}Pb (^{12}C, α)
$E_{^{12}C}$ = 187 MeV
dσ/dΩ (mb/sr)
1000
100
0
10
20
30
40
50
60
θ_{lab} (deg)
XBL 818-1160

Fig. 9

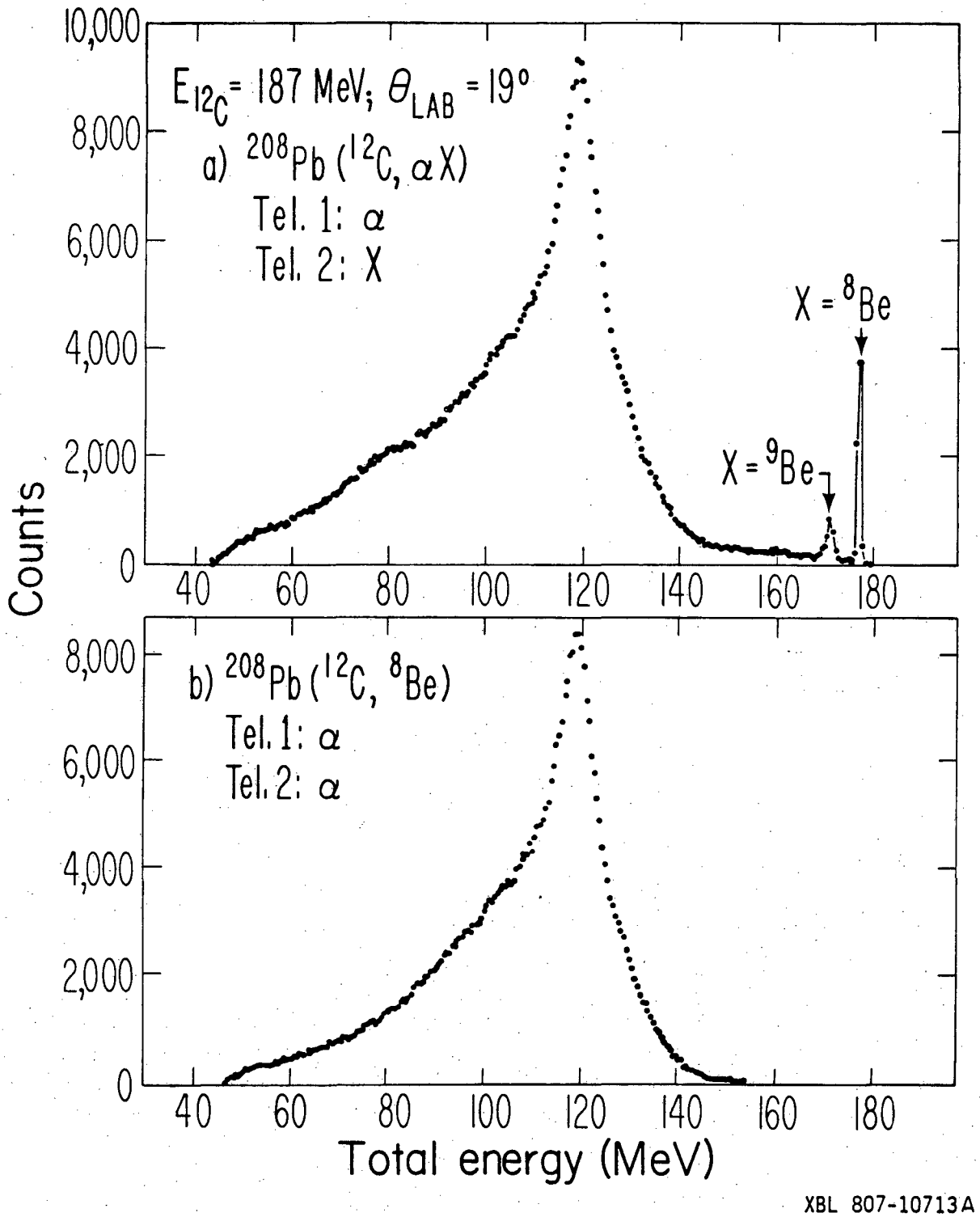

XBL 807-10713A

Fig. 10

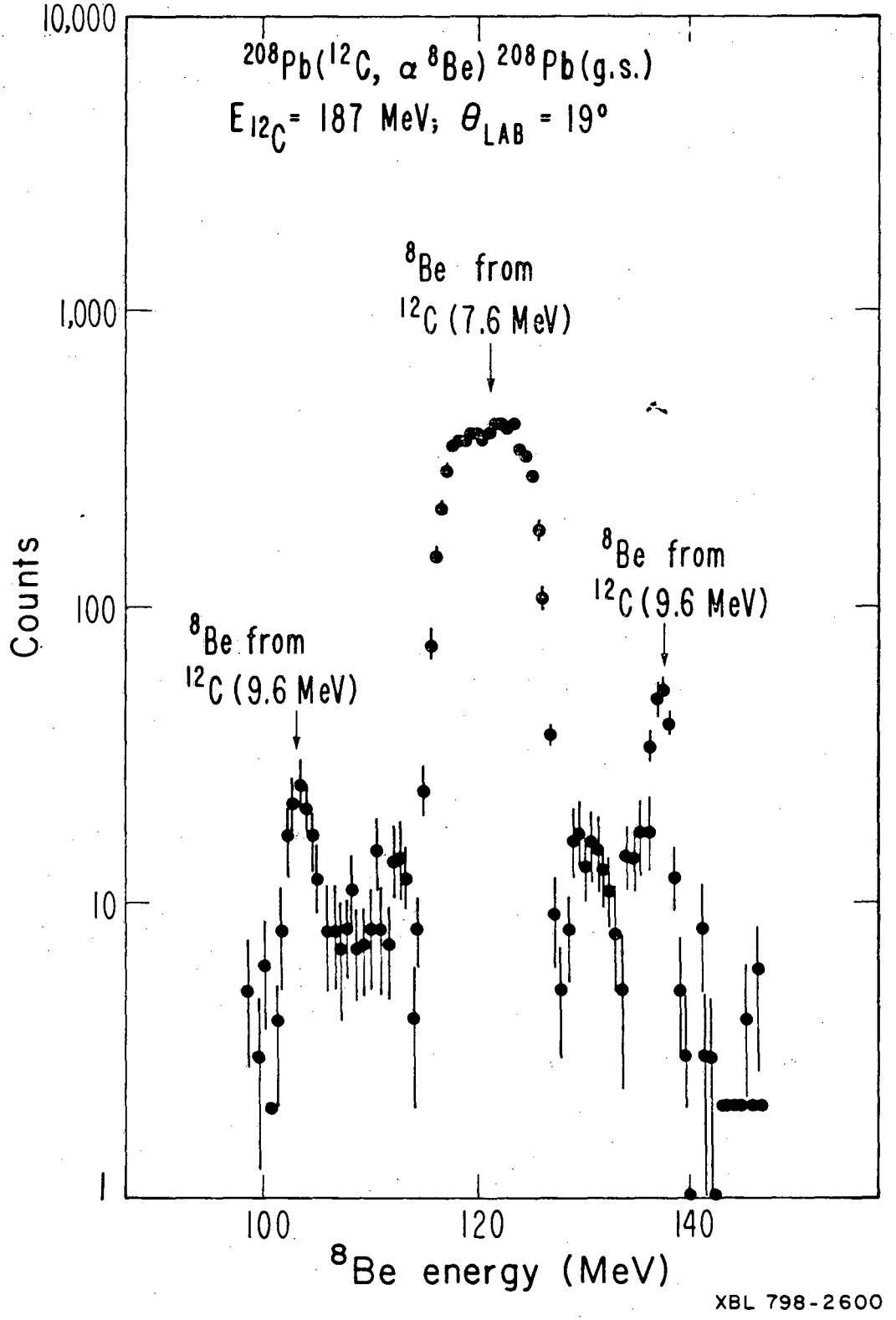
$^{208}Pb(^{12}C, \alpha\, ^{8}Be)\, ^{208}Pb(g.s.)$
$E_{^{12}C}$ = 187 MeV; θ_{LAB} = 19°
^{8}Be from ^{12}C (7.6 MeV)
^{8}Be from ^{12}C (9.6 MeV)
^{8}Be from ^{12}C (9.6 MeV)
Counts
10,000
1,000
100
10
1
100
120
140
^{8}Be energy (MeV)
XBL 798-2600

Fig. 11

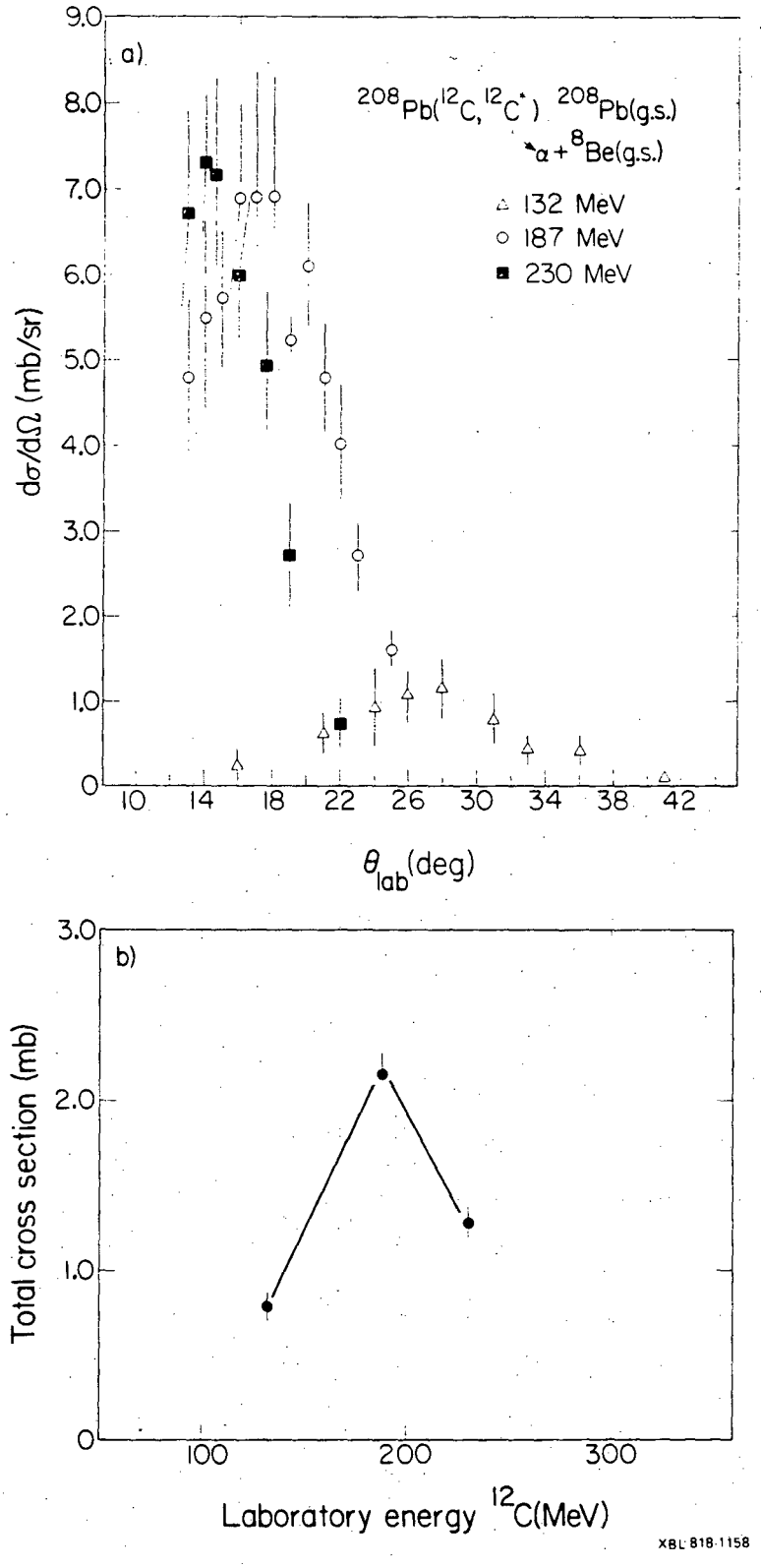
a)
$^{208}Pb(^{12}C,^{12}C^{*})\ ^{208}Pb(g.s.)$
$\alpha + ^{8}Be(g.s.)$
132 MeV
187 MeV
230 MeV
$d\sigma/d\Omega$ (mb/sr)
θ_{lab}(deg)
b)
Total cross section (mb)
Laboratory energy ^{12}C(MeV)
XBL 818-1158

Fig. 12

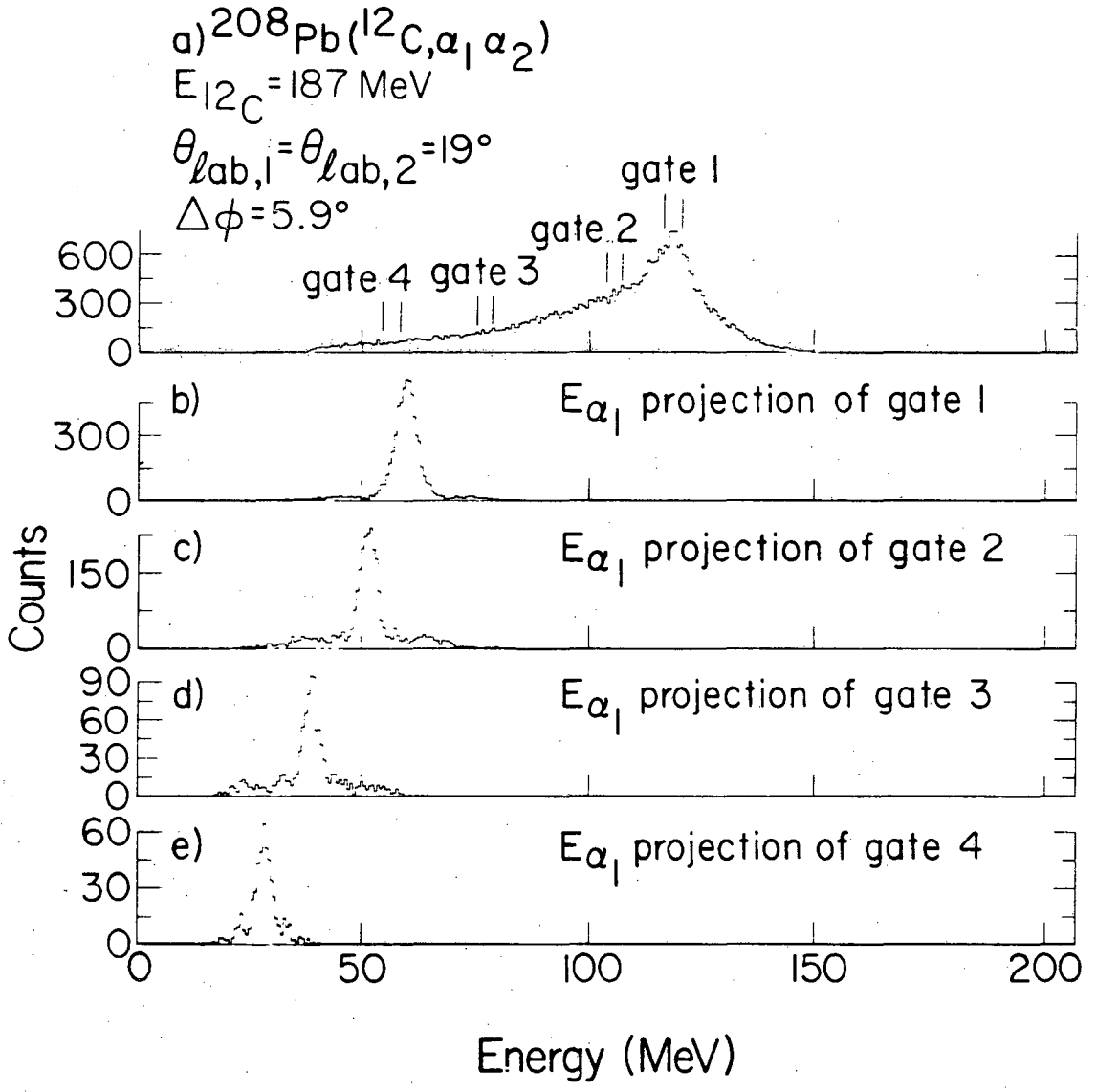
a) $^{208}Pb(^{12}C,\alpha_1\alpha_2)$
$E_{^{12}C}$=187 MeV
$\theta_{\ell ab,1}=\theta_{\ell ab,2}$=19°
$\Delta\phi$=5.9°
gate 1
gate 2
gate 3
gate 4
b) E_{α_1} projection of gate 1
c) E_{α_1} projection of gate 2
d) E_{α_1} projection of gate 3
e) E_{α_1} projection of gate 4
Counts
Energy (MeV)
XBL 818-1163

Fig. 13

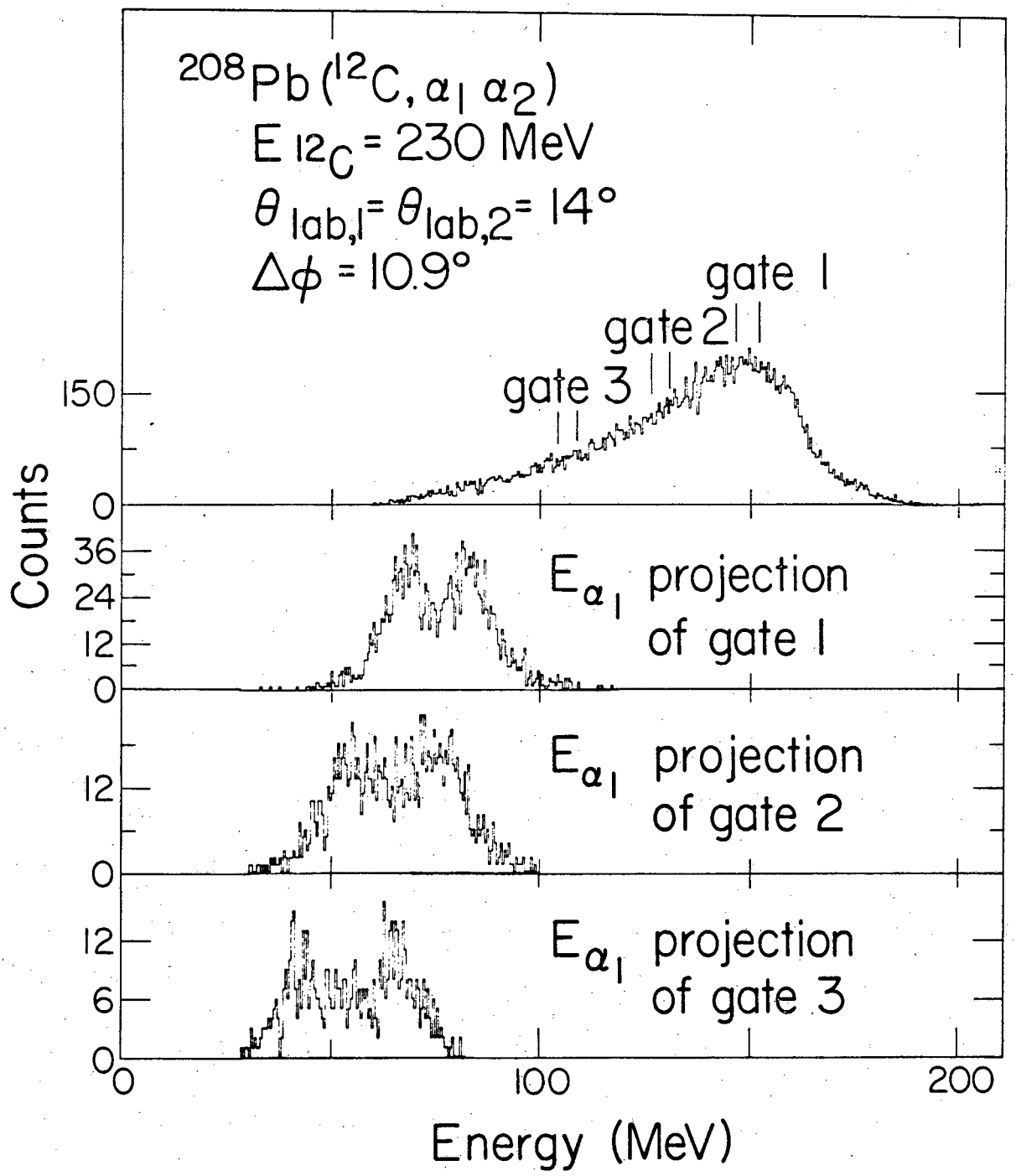
$^{208}Pb(^{12}C, \alpha_1 \alpha_2)$
$E_{^{12}C} = 230$ MeV
$\theta_{lab,1} = \theta_{lab,2} = 14°$
$\Delta\phi = 10.9°$
gate 1
gate 2
gate 3
Counts
150
0
36
24
12
0
E_{α_1} projection of gate 1
12
0
E_{α_1} projection of gate 2
12
6
0
E_{α_1} projection of gate 3
0
100
200
Energy (MeV)
XBL 819-7306

Fig. 14

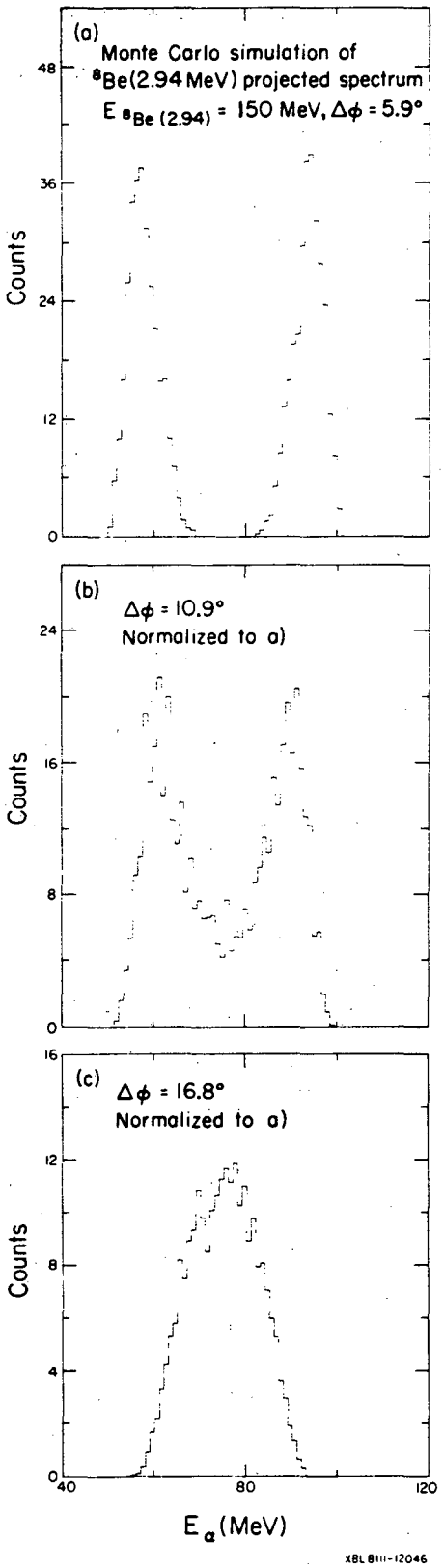
(a)
Monte Carlo simulation of
^{8}Be(2.94 MeV) projected spectrum
$E_{^{8}Be\,(2.94)}$ = 150 MeV, $\Delta\phi$ = 5.9°
Counts
48
36
24
12
0
(b)
$\Delta\phi$ = 10.9°
Normalized to a)
Counts
24
16
8
0
(c)
$\Delta\phi$ = 16.8°
Normalized to a)
Counts
16
12
8
4
0
40
80
120
E_{α} (MeV)
XBL 8111-12046

Fig. 15

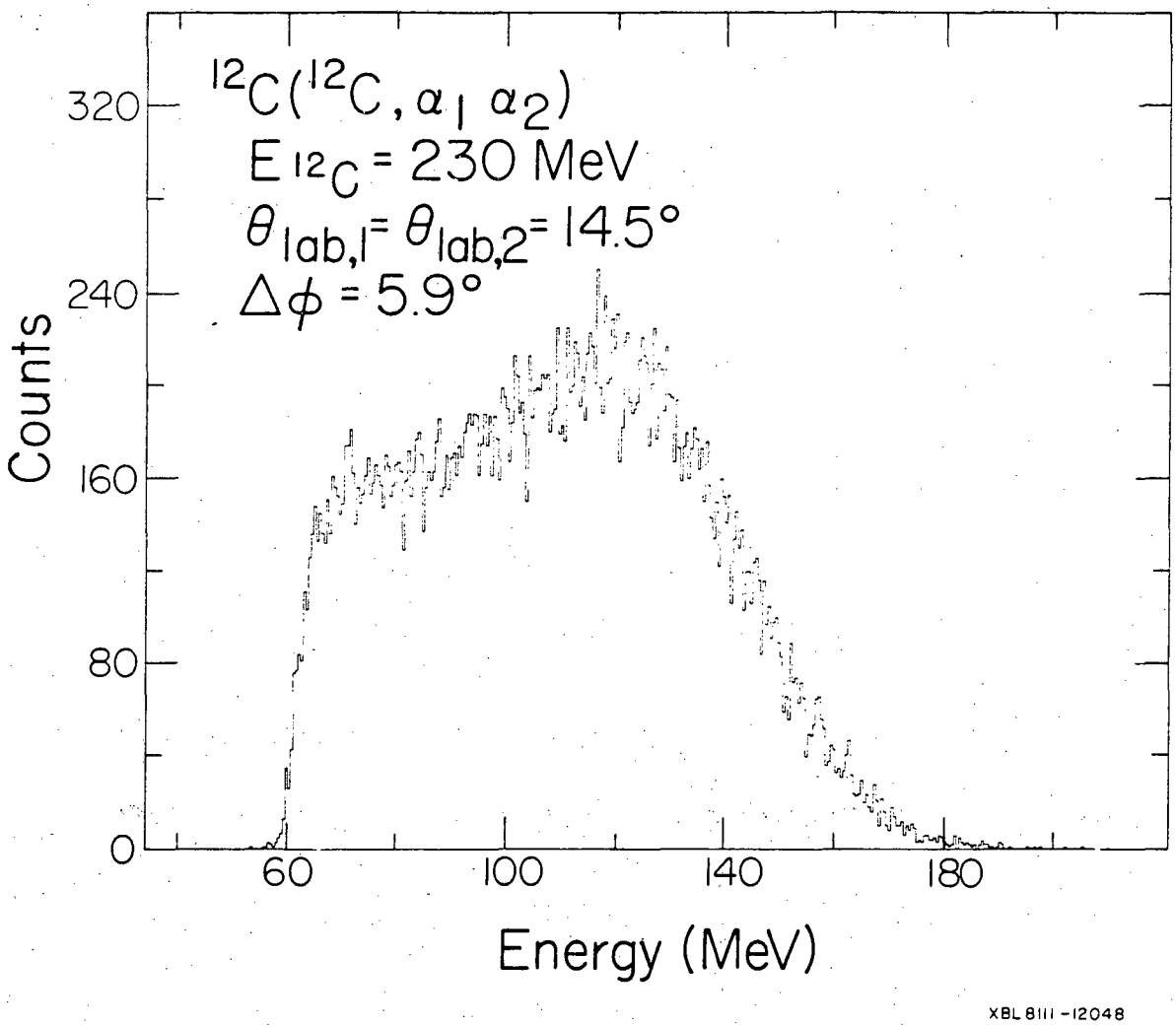
$^{12}C(^{12}C, \alpha_1 \alpha_2)$
$E_{^{12}C}$ = 230 MeV
$\theta_{lab,1} = \theta_{lab,2}$ = 14.5°
$\Delta\phi$ = 5.9°
Counts
320
240
160
80
0
60
100
140
180
Energy (MeV)
XBL 8111-12048

Fig. 16

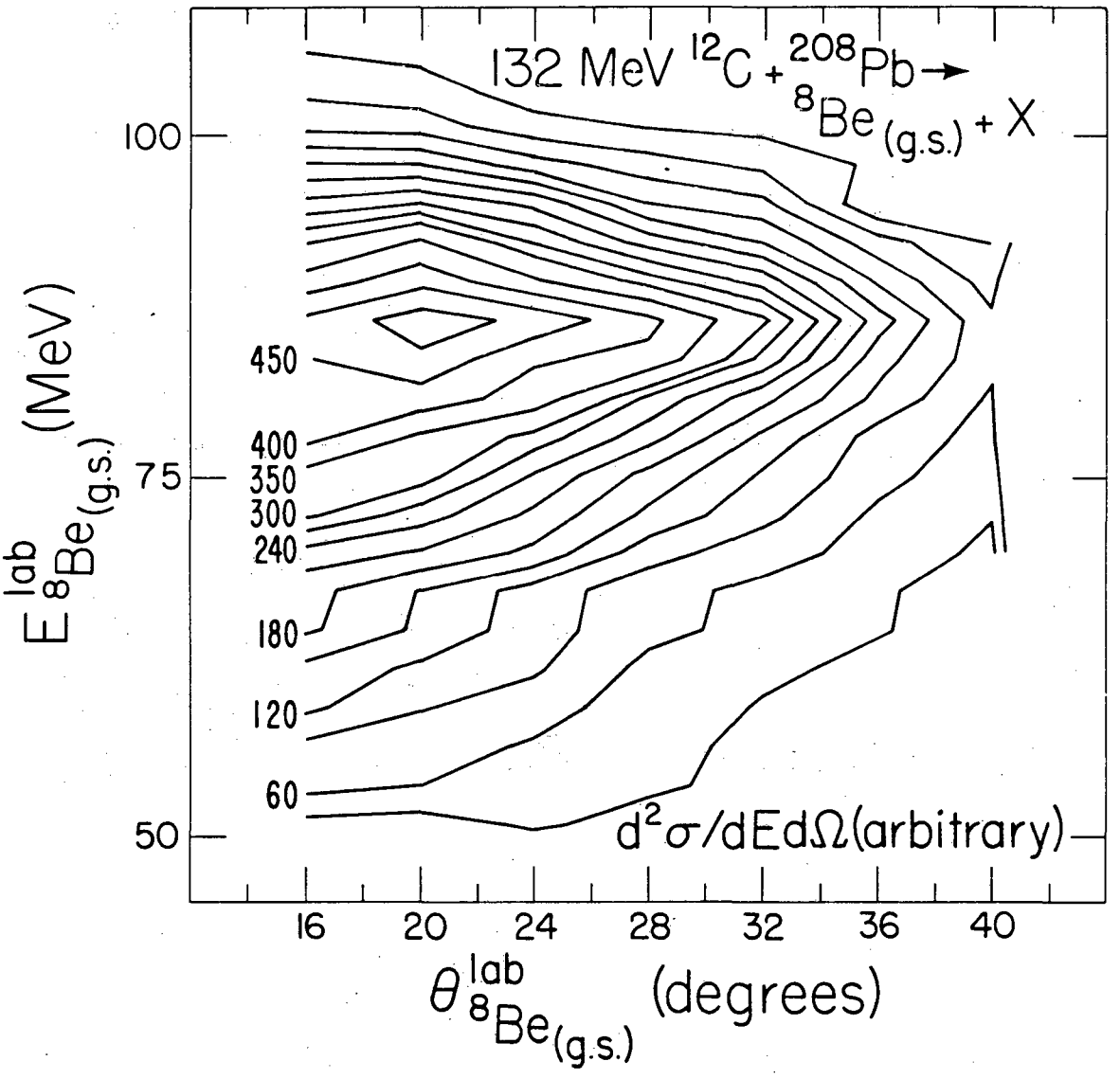
132 MeV $^{12}C + ^{208}Pb \rightarrow$
$^{8}Be_{(g.s.)} + X$
100
75
50
450
400
350
300
240
180
120
60
$d^2\sigma/dEd\Omega$(arbitrary)
$E^{lab}_{^{8}Be_{(g.s.)}}$ (MeV)
16
20
24
28
32
36
40
$\theta^{lab}_{^{8}Be_{(g.s.)}}$ (degrees)
XBL 8111-12003

Fig. 17

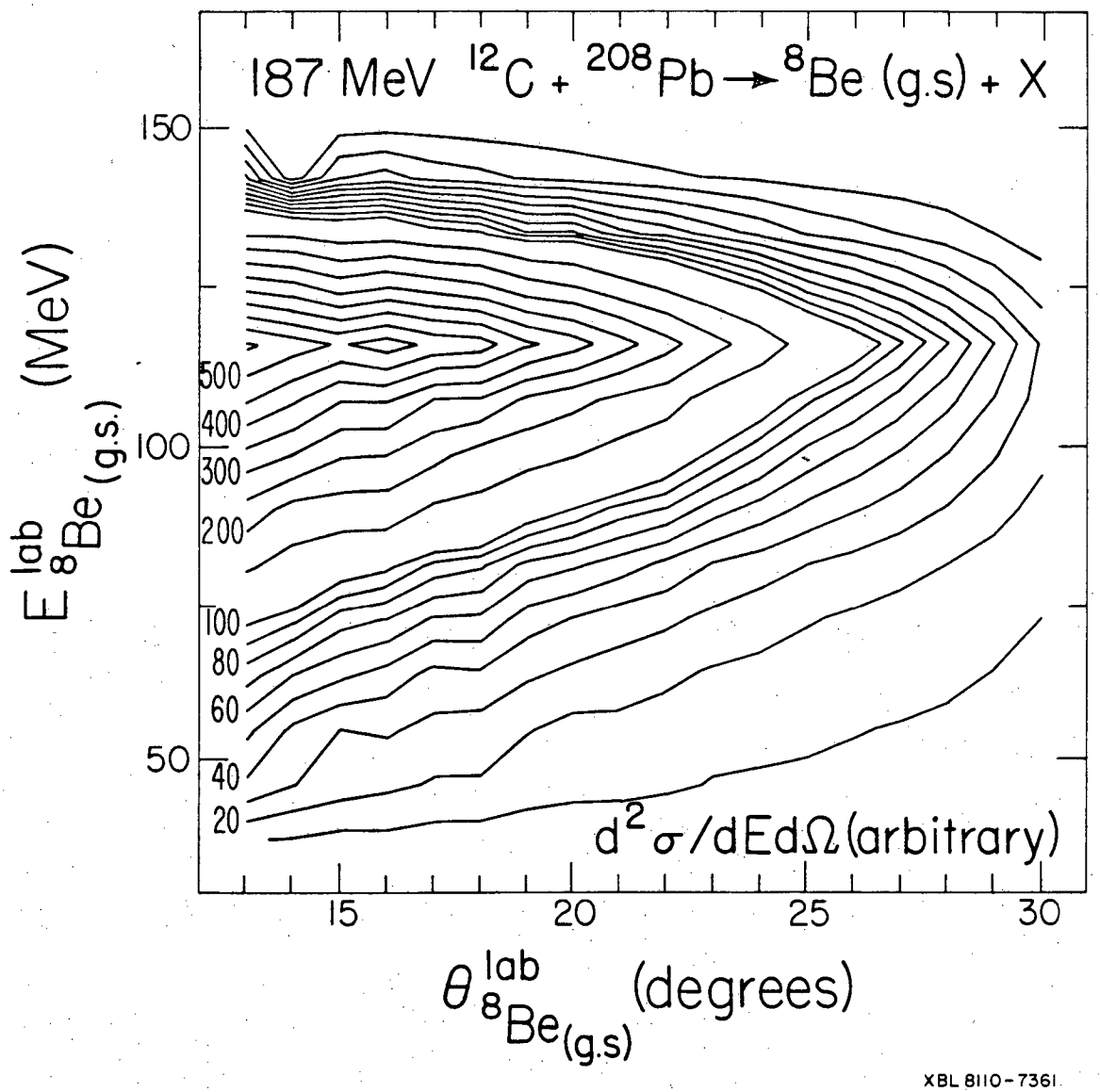
187 MeV $^{12}C + ^{208}Pb \rightarrow ^{8}Be$ (g.s) + X
150
100
50
500
400
300
200
100
80
60
40
20
$d^2\sigma/dEd\Omega$ (arbitrary)
15
20
25
30
$E^{lab}_{^8Be\,(g.s.)}$ (MeV)
$\theta^{lab}_{^8Be(g.s)}$ (degrees)
XBL 8110-7361

Fig. 18

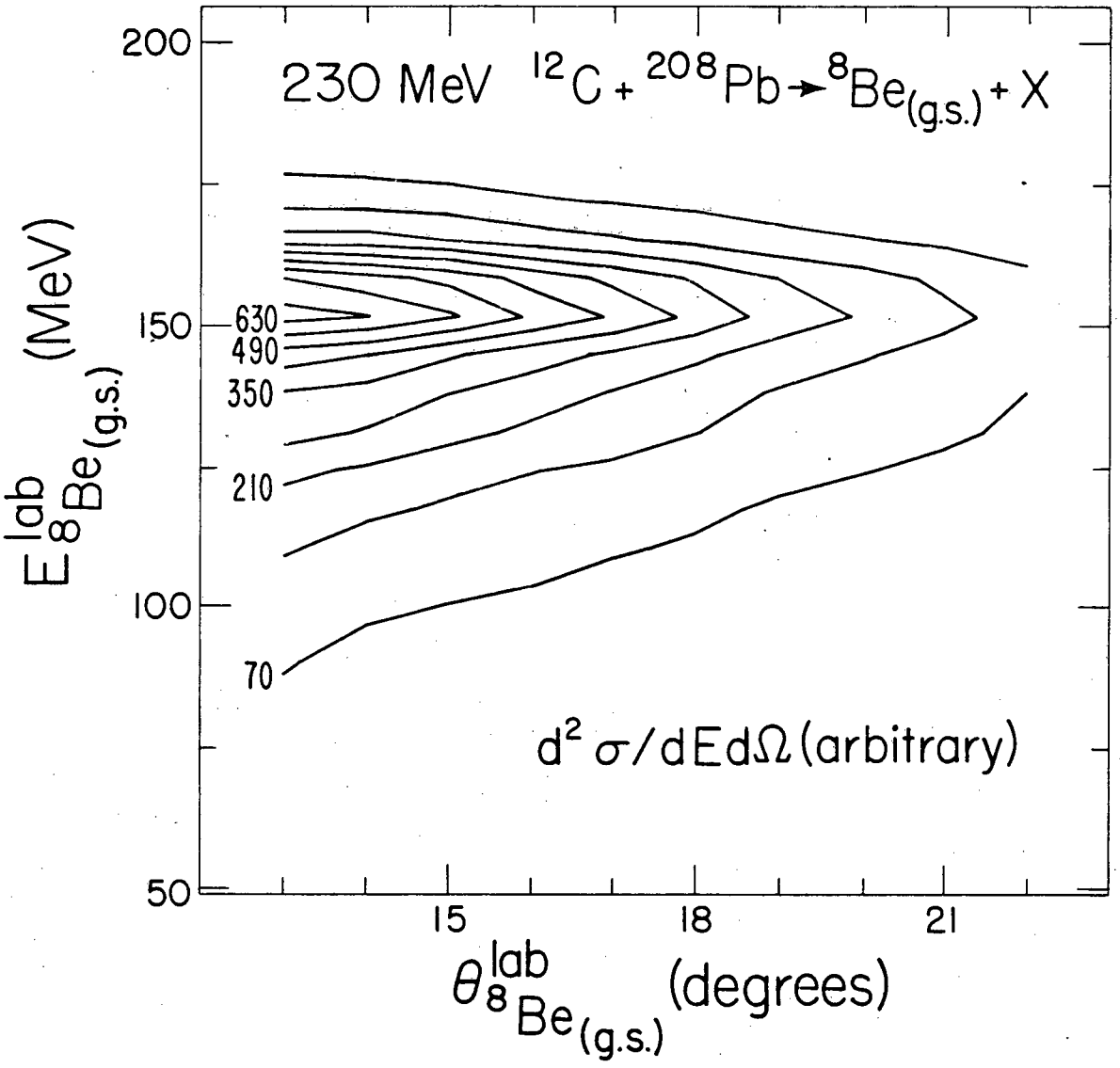
230 MeV $^{12}C + ^{208}Pb \rightarrow ^{8}Be_{(g.s.)} + X$
$E^{lab}_{^8Be_{(g.s.)}}$ (MeV)
200
150
100
50
630
490
350
210
70
$d^2\sigma/dEd\Omega$ (arbitrary)
15
18
21
$\theta^{lab}_{^8Be_{(g.s.)}}$ (degrees)
XBL 8110-12002

Fig. 19

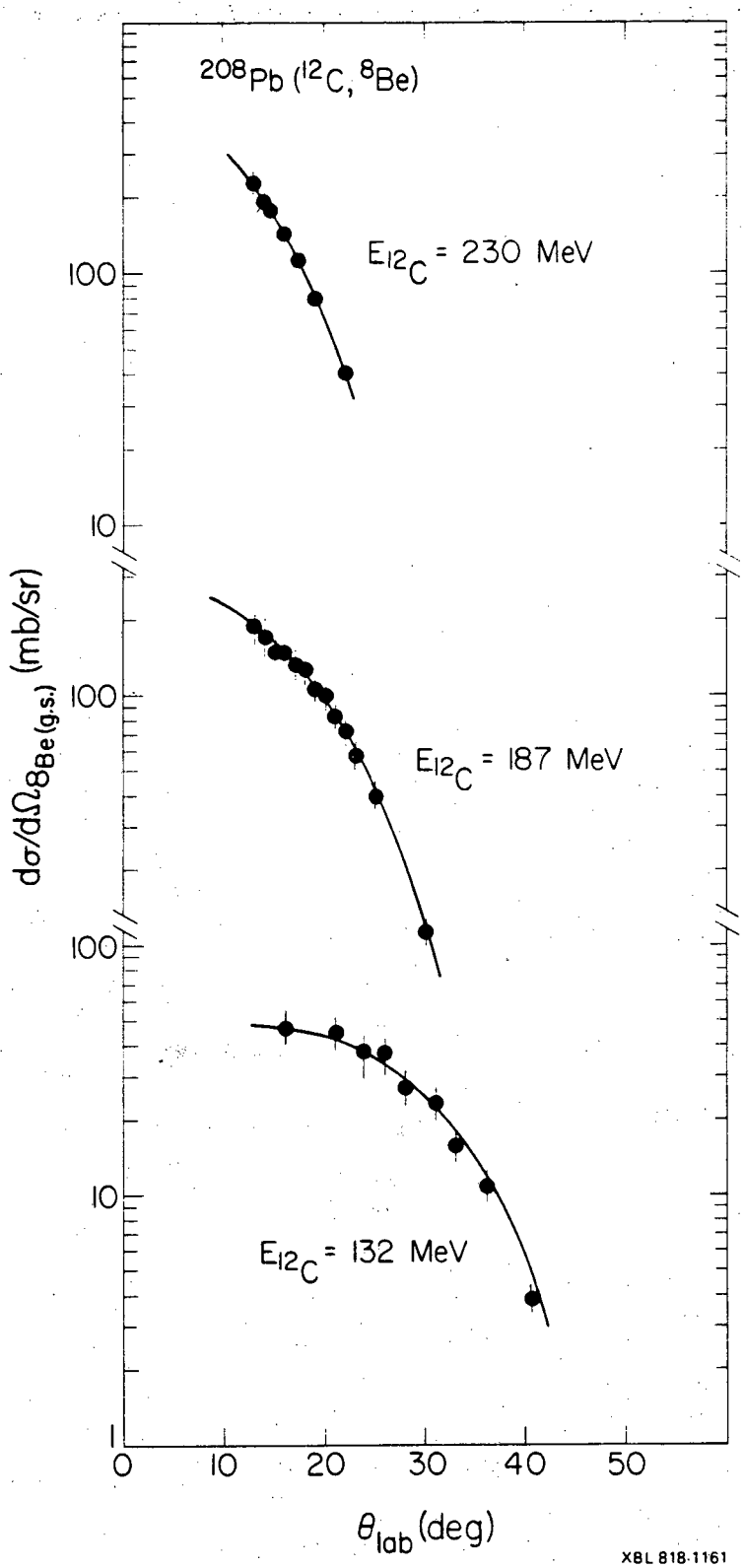
^{208}Pb (^{12}C, ^{8}Be)
$E_{^{12}C}$ = 230 MeV
$E_{^{12}C}$ = 187 MeV
$E_{^{12}C}$ = 132 MeV
$d\sigma/d\Omega_{^{8}Be(g.s.)}$ (mb/sr)
θ_{lab} (deg)
100
10
100
10
1
0
10
20
30
40
50
XBL 818-1161

Fig. 20

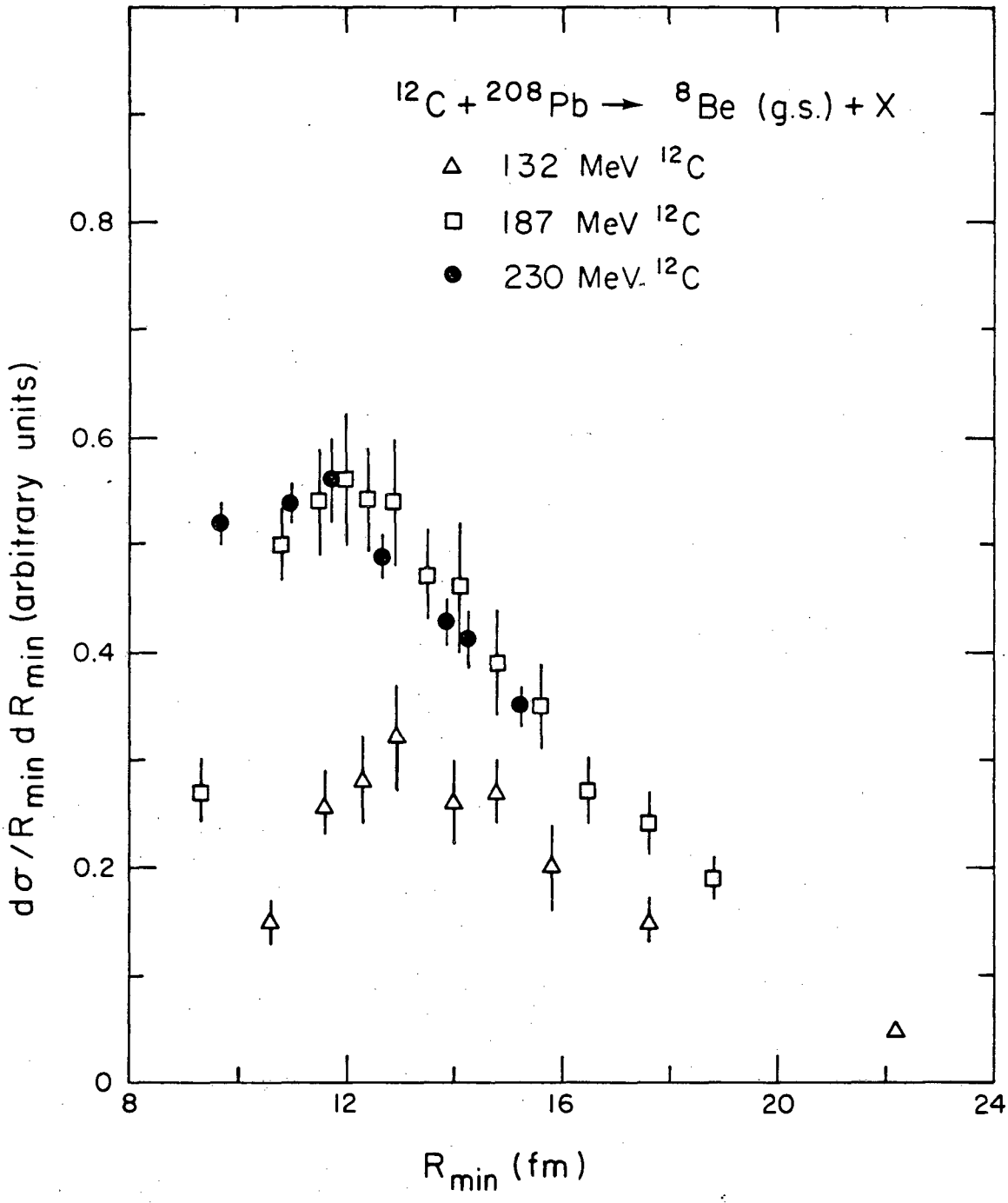

XBL 8110-7307

Fig. 21

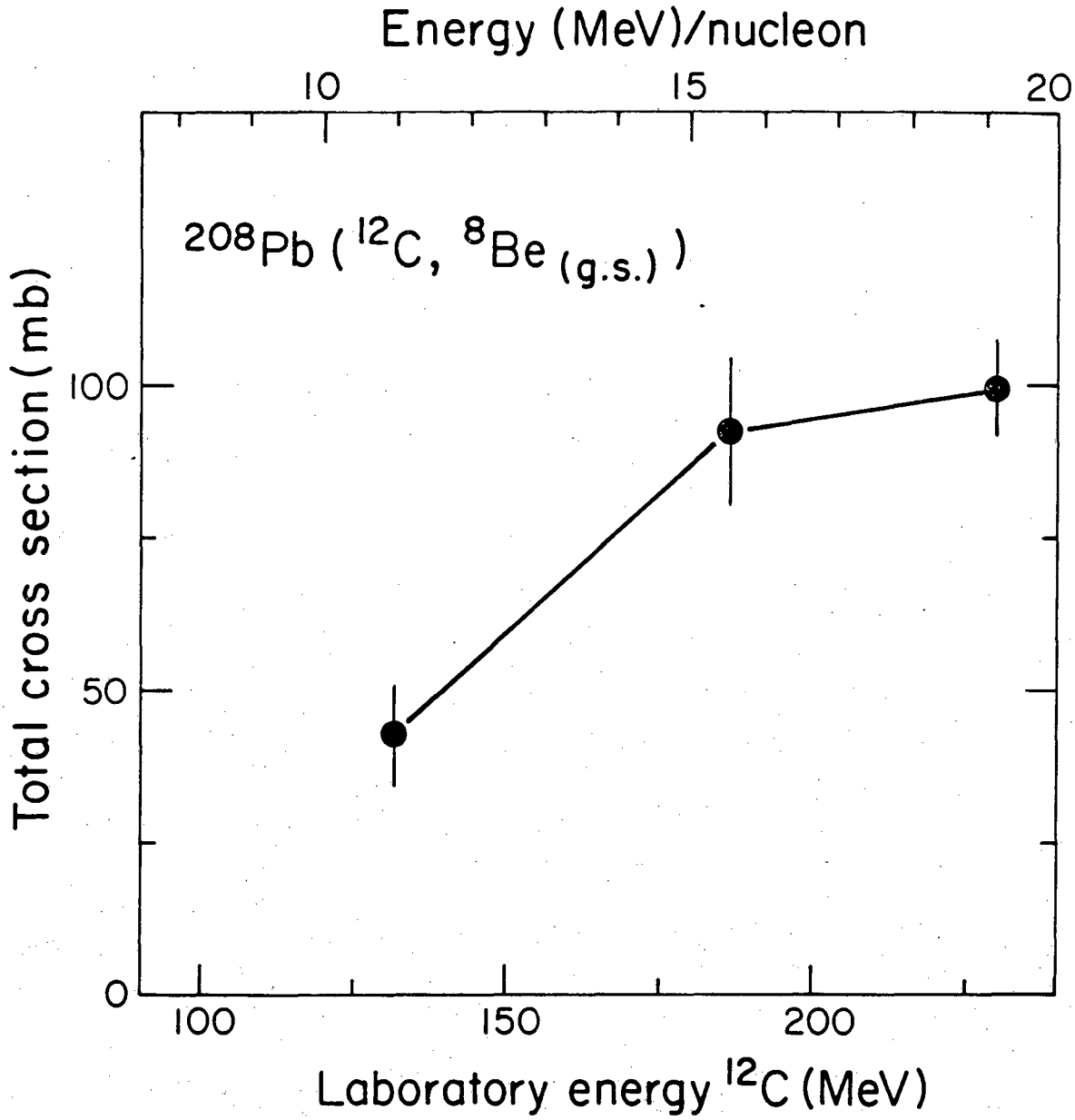
Energy (MeV)/nucleon
10
15
20
^{208}Pb (^{12}C, $^{8}Be_{(g.s.)}$)
Total cross section (mb)
100
50
0
100
150
200
Laboratory energy ^{12}C (MeV)
XBL8110-7398

Fig. 22

This report was done with support from the Department of Energy. Any conclusions or opinions expressed in this report represent solely those of the author(s) and not necessarily those of The Regents of the University of California, the Lawrence Berkeley Laboratory or the Department of Energy.

Reference to a company or product name does not imply approval or recommendation of the product by the University of California or the U.S. Department of Energy to the exclusion of others that may be suitable.

TECHNICAL INFORMATION DEPARTMENT
LAWRENCE BERKELEY LABORATORY
UNIVERSITY OF CALIFORNIA
BERKELEY, CALIFORNIA 94720